Guidance for estimating the blast load from vapour cloud explosions in traffic environments using the multi-energy method

Journal of Safety Science and Resilience 7 (2026) 100222

Contents lists available at ScienceDirect

Journal of Safety Science and Resilience

journal homepage: www.keaipublishing.com/en/journals/journal-of-safety-science-and-resilience/

Guidance for estimating the blast load from vapour cloud explosions in traffic environments using the multi-energy method

Fabio Lozano [a,*], Morgan Johansson [a,b], Joosef Leppänen [a], Mario Plos [c]

[a] Division of Structural Engineering, Chalmers University of Technology, Gothenburg, SE, 41296, Sweden
[b] Norconsult Sverige AB, Gothenburg, SE, 41755, Sweden
[c] Swedish Transport Administration, Gothenburg, SE, 41104, Sweden

ARTICLE INFO

Keywords:
Vapour cloud explosions
Traffic environments
Blast strength
TNO Multi-Energy Method
Computational fluid dynamics

ABSTRACT

The accidental release of a flammable gas on a road can result in a vapour cloud explosion (VCE). Such VCEs generate a blast wave that propagates away from the explosion, potentially damaging nearby structures. The TNO Multi-Energy Method is commonly used for a simplified estimate of the blast load resulting from a VCE. The method characterises the severity and duration of the blast wave using a case-specific strength class and combustion energy (which the method relates to the gas volume of the equivalent blast source). However, no specific guidelines for estimating the strength class in urban roads or related settings (such as carparks) are currently available in the literature. This makes implementing the method in such scenarios challenging and imprecise. The authors' work used computational fluid dynamics (CFD) to evaluate multiple gas explosion scenarios and proposed recommendations for determining the strength class and gas volume at the blast source. These scenarios comprised a group of vehicles engulfed by a stoichiometric propane-air cloud. It was concluded that the strength class could be reasonably estimated based on the number of vehicles in the transverse direction. Furthermore, the guidance for estimating the gas volume at the equivalent blast source was based on the critical gas volume, after which no further enhancement of overpressure was obtained. The recommendations were implemented in several scenarios and compared with corresponding CFD analyses. The results showed very good agreement for predicting impulse. Predicting overpressure was affected by the inherent asymmetry of the scenarios, although it was possible to achieve acceptable and conservative results.

1. Introduction

The accidental release of a flammable gas during transport may lead to catastrophic events such as jet fires, flash fires, boiling liquid expanding vapour explosions (BLEVEs) or vapour cloud explosions (VCEs). Liquified petroleum gas (LPG) and liquified natural gas (LNG) are two examples of flammable gases transported in large volumes with relatively high frequency. The inland transport of flammable gases is commonly carried out by road or railway, often coming near or passing through urban areas. Over the last century, there have been numerous accidents involving the land transport of flammable gases [1–3]. A notable accident involving an LPG road tanker occurred in 2020 in Wenling, China [4–6]. The tanker collided with a concrete guardrail, causing a cold BLEVE. This was followed by a major release of LPG, which dispersed into the surrounding areas, forming a large vapour cloud. The cloud eventually ignited and developed into a powerful VCE. This disaster resulted in 20 fatalities, 175 injuries and significant damage to buildings and infrastructure. The accidents in Kerala (India) in 2012 [7] and Bologna (Italy) in 2018 [8,9] are two other recent disasters with devastating consequences related to the transport of LPG close to urban areas. This highlights the importance of investigating the effects of accidental explosions when transporting flammable gases in urban environments.

Among the potential consequences of an accidental release during transport, a VCE is often regarded as the most likely event [10,11]. A VCE is a violent combustion of a premixed cloud of flammable gas and air. Such a cloud may form due to the combination of unintended release and delayed ignition, enabling the flammable gas to mix with the

Peer review under the responsibility of China Science Publishing & Media Group Ltd.
* Corresponding author.
E-mail address: fabio.lozano@chalmers.se (F. Lozano).

https://doi.org/10.1016/j.jnlssr.2025.100222
Received 18 January 2025; Received in revised form 15 April 2025; Accepted 23 April 2025
Available online 22 June 2025

surrounding air. VCEs may result in loss of life and extensive damage due to the high temperature and overpressure[1] generated. Two important factors influencing the strength[2] of a VCE are congestion and confinement of the gas cloud. Congestion in the flame path will generate turbulence, which in turn accelerates the flame, resulting in increased overpressure. Confinement also contributes to pressure build-up by limiting the free expansion of the flow [12]. A gas cloud in a traffic environment[3] may come across regions which are partly confined (such as regions under and between vehicles) or congested (such as obstructions caused by vehicle wheels). Thus, both confinement and congestion may lead to pressure build-up in the event of a flammable gas cloud ignition on the road.

VCEs produce a blast wave that propagates outwards from the centre of the explosion. The severity of the blast wave depends on the strength of the explosion. The arrival of the blast wave at a given point is characterised by a major, rapid increase of pressure, followed by a rarefaction wave. Structures near roads on which the transport of flammable gasses is permitted may be outside the explosion area and yet be affected by the ensuing blast wave. Hence, when designing or verifying the capacity of these structures, it is often necessary to estimate the characteristics of a blast wave impinging on them. This involves estimating blast wave parameters such as peak overpressure, peak impulse, positive-phase duration and the shape of the overpressure-time history. Once the blast load has been defined, different approaches with different degrees of complexity can be used to assess the response of the structure, from simplified single-degree-of-freedom (SDOF) models to robust finite element (FE) models that account for fluid-structure interaction. At a component level, approaches based on overpressure-impulse diagrams (PI diagrams) are also commonly used to predict the dynamic response and damage of the blast-loaded structure [13,14]. The advantage of this method is that a given blast-loading scenario can be defined solely by the peak overpressure and impulse acting on the structural element in question.

An essential part of defining the resulting blast load is the accurate estimation of the strength of the VCE and the amount of combustion energy released by the source of the strong blast. Such a task may be accomplished with the help of computational fluid dynamics (CFD) codes, which solve the Navier-Stokes equations for compressible fluid flow, plus numerical models for combustion and turbulence. Over the last two decades, CFD codes have been used extensively to analyse flammable gas explosions [15]. A comprehensive review of the recent usage and development of CFD methods within this field can be found in [16–18]. Most of the published research works have focused on applications within the context of the process industry, including the evaluation of vapour cloud dispersion and explosion in industrial parks and offshore modules [19–22], evaluation of the effect of obstacles [23–25], vented explosions [26–29] and propagation of the ensuing blast wave [30–32]. However, compared to applications in the process industry, relatively few studies have focused on gas explosions in traffic scenarios. Furthermore, most of these studies are concerned with gas explosions in vehicular tunnels [33–37] and refuelling stations [38–40]. There are very few available examples of studies of VCEs in open traffic environments in which vehicles are the main (or only) source of confinement and congestion [39,41].

Lozano [41] investigated the strength of gas explosions in an open-road environment using CFD analysis. Several scenarios were studied, comprising a group of vehicles with different configurations engulfed by a propane-air cloud with stoichiometric concentration. The study employed a factorial analysis to investigate the effect on the resulting blast strength of various parameters related to the configuration's geometry. Parameters of interest included the number and layout of vehicles, distance between vehicles, gas volume and location of the ignition point. The study concluded that the number of vehicles in the direction perpendicular to the direction of traffic had the greatest effect on the resulting overpressure. However, the work in [41] was limited to studying the blast strength. Moreover, the range over which the parameters of interest varied was limited. Hence, further investigation is needed, including an investigation of the combustion energy at the source of the strong blast.

Evaluation of VCEs with CFD calculations is not problem-free. Firstly, CFD tools require specialised knowledge to produce useful results. Additionally, CFD calculations are often resource-intensive and time-consuming. This means that CFD calculations may not be easily accessible, suitable or even desirable in many situations, particularly in the early design stage of a given project. Hence, there is a need for faster and simpler methods of estimating the blast load due to gas explosions, which can still produce sufficiently accurate results.

Some simplified methods of estimating VCE blast loads are currently available. These have been developed based on experimental observations or numerical simulations. Examples of such methods include the TNO Multi-Energy Method (MEM) [42], the Baker-Strehlow-Tang (BST) method [43,44] and the Congestion Assessment Method [45]. Common to all these methods is that the user must estimate the strength at the source of the blast, arguably the most challenging aspect of such simplified methods. Other practical methods have been developed for specific conditions, such as gas explosions in unconfined environments [46–48], gas explosions in tunnel-like environments [49] or vented explosions [50–52]. However, such methods have limitations concerning, for instance, the geometry of the environment, mixture characteristics, or total gas volume, and cannot be easily extrapolated to other settings.

Among the different simplified methods, the MEM is one of the most extensively used due to its coherent theoretical background and relative simplicity. The method builds on the fact that a strong blast can only arise in those regions of a flammable gas cloud that are partially congested or confined (referred to here as *blast sources*). The contribution to blast generation of the remaining, unconfined part of the cloud is presumed negligible. The method provides charts for side-on overpressure and positive-phase duration as a function of the stand-off distance and strength class of the explosion, ranging from 1 (weak deflagration) to 10 (detonation). The distance is scaled based on the energy of the blast source. More information about the MEM is provided in Appendix A. Guidelines for determining the strength class number can be found in the literature, [53–55] for example. Correlations have also been proposed [54–57] to calculate the maximum overpressure for some specific conditions based on experiments or numerical analyses. However, such guidelines are primarily intended for applications in process industry sites, which makes their implementation for explosion scenarios in traffic environments unclear and ambiguous. Currently, when using the method in traffic-related situations, users are forced to adapt the existing guidelines based on their own experience and judgement, which introduces an additional measure of uncertainty into the design process. One consequence of this is that different evaluations of VCEs in traffic environments sharing similar conditions may result in different blast load characteristics, even within the framework of the same project [58]. Therefore, more effective recommendations are needed for utilising the MEM to predict the blast load generated by VCEs in traffic environments.

This article aims to develop recommendations for selecting a strength class and estimating the combustion energy at the source of a strong blast when applying the MEM to gas explosion scenarios in traffic environments. The intention is to pave the way for a more uniform and predictable estimate of the blast load from VCEs in urban road settings

[1] Overpressure is defined as the difference between the absolute pressure and the ambient pressure.

[2] The term *strength* relates to the overpressure generated by the explosion.

[3] The term *traffic environment* refers to settings on or near a road, on which a group of vehicles is likely to be present in the event of an accidental release of a flammable gas during transport. Examples of traffic environments include congested roads, open carparks near the road and refuelling stations.

using the MEM. The overarching aim is to facilitate the estimation of blast wave parameters when designing structures exposed to the risk of gas explosions in traffic environments (such as roads and carparks). The blast wave parameters of interest in this article are the peak overpressure and peak positive impulse. The study employed CFD calculations using FLACS-CFD [59]. Several open-area scenarios were analysed, comprising a group of vehicles engulfed by a stoichiometric mixture of propane and air. The influence of different geometrical parameters on the resulting explosion was also investigated. Parameters of interest included the number of vehicles in the transverse and longitudinal directions, the gas volume and the separation distance between vehicles.

2. Methodology

2.1. Overview

This work aims to develop guidelines for using the MEM to determine the blast load from VCEs in traffic environments. The traffic environment of interest is an open area in which a cluster of vehicles is engulfed by a flammable mixture of fuel and air. In this type of environment, vehicles are the main source of obstruction and confinement. That is, the group of vehicles is the assumed source of a strong blast. Two illustrations of the target scenario are given in Fig. 1. In the figure, the flammable gas leaking from a road tanker mixes with the surrounding air to form a flammable mixture, which covers stationary vehicles on (a) the road or (b) a nearby carpark.

The study was carried out using CFD calculations. Compared to an experimental campaign, this numerical approach is a relatively economical alternative that enables the evaluation of multiple scenarios and sampling of results across many more result points. A parametric study was initially conducted to investigate the effects of different geometrical parameters on the explosion strength. The parametric study was the basis of the initial concept formulation for addressing how to adapt the MEM to the environment of interest. Additional reference scenarios were subsequently analysed to fit the MEM (according to the general formulation devised in the initial stage) to the CFD calculation results. The performance of the proposed guidelines was then evaluated for multiple scenarios besides the reference cases. In addition to visual inspection, statistical performance indicators were implemented to evaluate the MEM predictions.

2.2. Parametrisation of the studied scenarios

Several simplifications were made for evaluating a gas explosion in the environment of interest. The most significant one concerns the shape and concentration of the gas cloud, which was assumed to be rectangular and uniform in concentration. Furthermore, to fit the MEM, only propane-air mixtures were considered. The primary reason for this choice is that LPG (comprising at least 95 % propane) is the most frequently transported fuel gas in Sweden and often serves as the basis for risk analyses related to the domestic transportation of flammable gases [60,61]. The mixture concentration that produces the maximum laminar burning velocity (equivalence ratio 1.05 for propane-air mixtures) was chosen. A few scenarios with methane-air mixtures were also investigated.

All vehicles were assumed to have equal shape and size, roughly representing a typical private car. The group of vehicles was assumed to be arranged in a rectangular pattern. All dimensions were rounded to a multiple of 50 mm to guarantee a perfect match between the geometry of the vehicles and the calculation grid. The global geometry of the scenario is defined by the five parameters listed in Table 1. Different scenarios were generated by varying these defining parameters. Fig. 2 shows a schematic representation of the gas cloud and configuration of the vehicle group, as well as the geometry of the mock-up vehicle. The studied scenarios are summarised in Appendix B. In all scenarios, the origin of the coordinate system was located at the outside corner of the bottom leftmost vehicle.

When performing the CFD analyses of these scenarios, the ignition point was placed at the edge of the congested region, which, according to [41], produces the greatest overpressure. It should be noted that the gas volume, as defined here, is used for CFD simulations. The gas volume used in the MEM may be smaller.

Table 1
Parameters for defining the studied scenarios.

Parameter	Description
A	Distance between vehicles.
B	Extension of the gas cloud in the horizontal plane outside the group of vehicles, measured from the edge of the group of vehicles.
C	Height of the gas cloud measured from the ground.
D	Number of vehicles in the transverse direction (*y*-direction in Fig. 2).
E	Number of vehicles in the longitudinal direction (*x*-direction in Fig. 2).

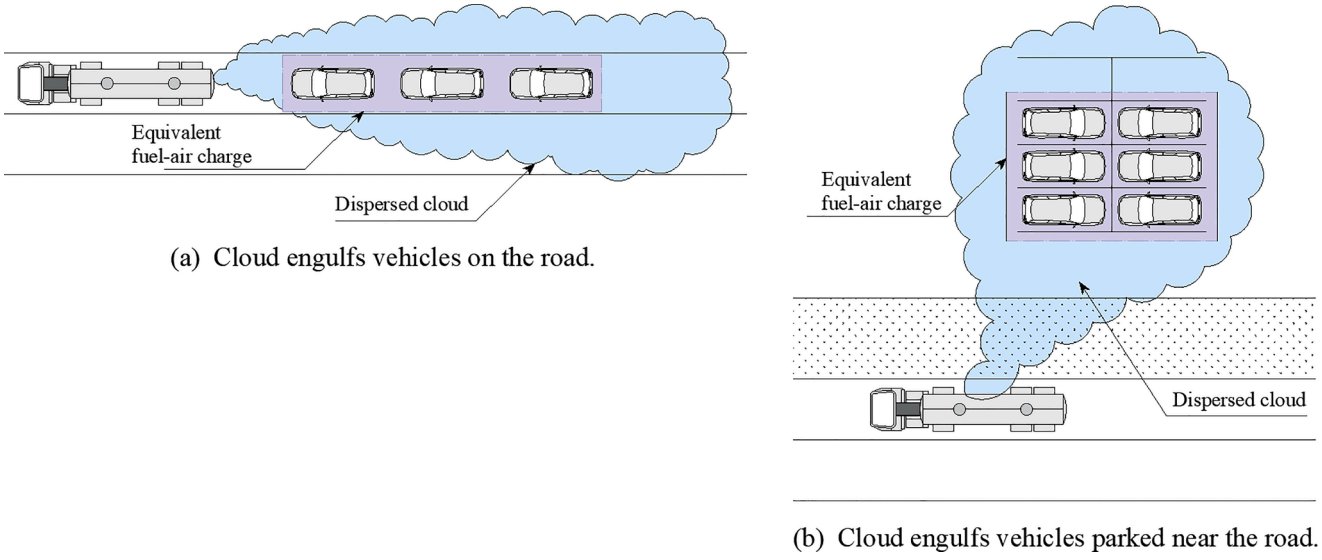

Fig. 1. Schematic examples of gas dispersion scenarios in a road environment relevant to the work in this article. The blue region is the actual dispersed cloud. The purple region is the equivalent blast source used in the MEM.

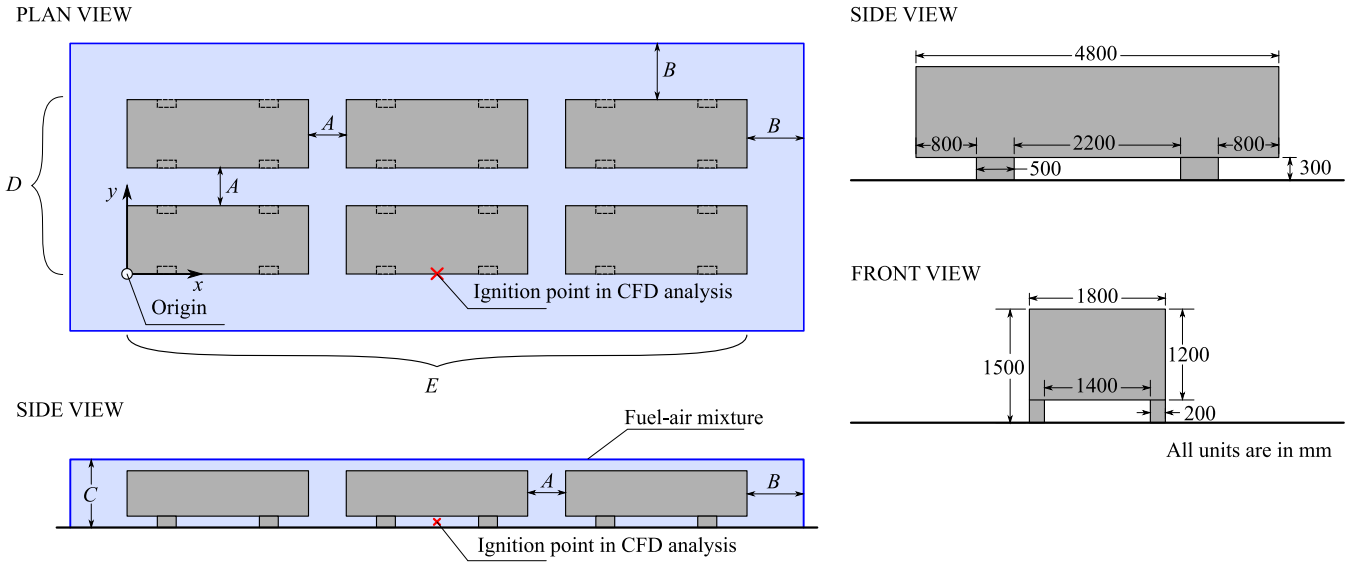

Fig. 2. Parameters defining the gas explosion scenarios and geometry of mock-up vehicle. The ignition point, marked with a red cross, is placed at 175 mm above ground.

2.3. CFD modelling

The CFD analysis of the studied scenarios was conducted with the finite volume code FLACS-CFD, v.22.1 [59]. A comprehensive description of the theoretical background of FLACS-CFD is given in [62–64]. Calculations with FLACS-CFD are performed on a structured Cartesian grid and rely on the Porosity Distributed Resistance approach in combination with several sub-grid models for consideration of the effects of sub-grid objects on turbulence generation and flame wrinkling. Turbulence is modelled with the standard k-ε turbulence model [65].

The calculation domain for all models consisted of a central *core domain* and an external *stretched domain*. 50 mm cubical cells were used within the core domain, with the vehicles and unburned gas cloud placed entirely inside it. In this domain, the grid was aligned to the edges of the vehicle's geometry. Thus, the porosity values in the studied scenarios were either 0 (completely blocked cell) or 1 (completely open cell). No intermediate porosity values existed anywhere in the models. In the stretched domain, the cell size was gradually increased by geometrical progression. Non-reflecting boundary conditions were used at all outlets. The ground and vehicles were modelled as rigid reflective surfaces. The Courant-Friedrich-Levy numbers were set to their default values (CFLC = 5 and CFLV = 0.05). Lastly, the STEP = "KEEP_LOW" option was used to ensure sufficiently short time steps in the later stages of the simulation. This prevented artificial numerical damping of the pressure waves.

As only results in the positive quadrant were of interest (see position of origin in Fig. 2), a sufficiently large core domain size was chosen to ensure that the flame front never left the core domain in the *positive* x and y directions. However, to decrease computational demands, the size of the core domain in the *negative* x and y directions was limited. The

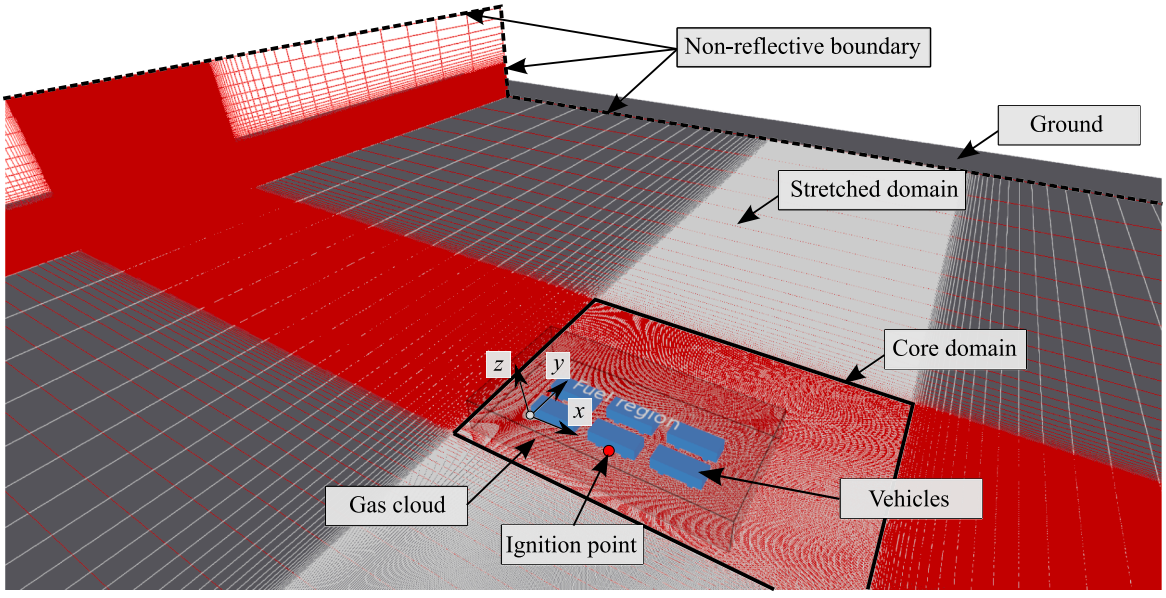

Fig. 3. Example of a CFD model with 2 × 3 vehicles.

effect of premature stretching of the grid towards the negative directions was investigated in a few scenarios and deemed to have little impact on the results in the region of interest. Fig. 3 depicts a sample model. Calculations were made in parallel, using 16 CPUs.

The initial turbulence conditions are described by the isotropic fluctuating velocity, u' and the turbulence length scale, l_{LT}. A value of u' = 1.0 m/s was judged in [41] to allow for conservative but realistic estimates in this type of environment. Therefore, u' = 1.0 m/s was used for all explosion scenarios in this study. The turbulence length scale was set to 50 % of the cell size in the core domain (25 mm).

Maximum overpressure results were stored for all cells. All other results were only stored at monitor points, arranged in a structured grid in the positive quadrant of the model space. The distance between monitor points is 1.0 m in the horizontal plane. In the vertical plane, the monitor points were created at 0.18 m and 1.48 m above ground.

2.4. Statistical performance indicators

Statistical performance indicators were used to conduct a more objective evaluation of the prediction with the MEM beyond what can be achieved solely by visual inspection. Two commonly used performance indicators were adopted: the mean bias (MG) and geometric variance (VG) [66–69]. MG is a measure of the systemic bias of the model, while VG facilitates the evaluation of both the systematic bias and the scatter of the model. These indicators are defined by Eqs. (1) and (2), in which a_o is the *observed* value and a_p is the corresponding *predicted* value. Results from the MEM were treated as *predicted* values, while those from the CFD analyses were treated as *observed* values. A perfect model would have MG and VG = 1.0. Values of MG greater than 1.0 indicate overprediction, while values less than 1.0 indicate underprediction.

$$\mathrm{MG} = \exp\left[\overline{\ln(a_p)} - \overline{\ln(a_o)}\right] \tag{1}$$

$$\mathrm{VG} = \exp\left[\overline{(\ln(a_p) - \ln(a_o))^2}\right] \tag{2}$$

These, among other performance indicators, are used by the CFD software developers in their validation studies. Therefore, the indicators could be used to ensure that the performance of the MEM compared to CFD calculations was within the confidence interval of the CFD results, as compared to experimental observations.

It should be noted that no true, random scatter is present in the studied models due to the numerical nature of both the *predicted* and *observed* values. However, scatter may still arise due to the contrast between the asymmetric configuration of the scenarios (which may cause a highly directional distribution of the overpressure) and the assumption of point-symmetry intrinsic to the MEM.

Acceptance criteria in terms of these statistical indicators have been proposed by several authors [66,68,69]. The target acceptance criteria adopted here are ±30 % for the mean bias (which corresponds to $0.7 < \mathrm{MG} < 1.3$) and a scatter factor of about two from the mean (which corresponds to approximately $\mathrm{VG} < 1.6$). Where relevant, the subscripts $_p$ and $_i$ are used to distinguish between overpressure and impulse predictions.

3. Parametric study

Before formulating an approach for implementing the MEM in a traffic environment, it is of interest to investigate the effect of the defining parameters from Table 1 on the resulting explosion. This was achieved by conducting one-factor-at-a-time analyses, whereby the influence of each of the defining parameters was studied by fixing all other parameters and varying only the parameter of interest. The ultimate purpose of this study was to identify the most significant relationships between the defining parameters and the inputs required for using the MEM.

The effects of multiple parameters on the maximum overpressure at the centre of a blast in a traffic environment were previously investigated by Lozano [41] using the principles of factorial design. That study focused on the efficient and economical simultaneous examination of multiple parameters to identify the most significant effects and interactions. However, the conducted factorial analyses were limited by the fact that the parameters were varied over two or three different levels to restrict the number of possible combinations. The one-factor-at-a-time analyses presented in this article focused instead on investigating more levels per factor at the expense of disregarding most interaction effects. Similarities and differences between the work conducted here and the results reported in [41] are highlighted where relevant.

The base scenario for the one-factor-at-a-time study was defined by the input parameters: $A = 0.5$ m, $B = 1.0$ m, $C = 1.8$ m, and $D = E = 3$. Starting from this base scenario, each parameter was varied over at least five levels while keeping the other parameters constant. A total of 38 scenarios were investigated, as described in Table B.1. In all scenarios, the ignition point was placed at the edge of the configuration.

3.1. Effect of the separation distance between vehicles

Fig. 4 shows the effect of the separation distance between vehicles (parameter A) on the maximum overpressure. Clearly, there is a critical value for which the explosion strength is greatest. If A is smaller than the critical value, increasing the distance between vehicles results in greater overpressure. Conversely, if A is greater than the critical value, increasing A results in decreased maximum overpressure. These results agree with the numerical results reported in [41]. Similar observations from an experimental study of the explosion of a methane-air mixture in a tube with two obstacles were reported in [70].

The geometry of the vehicle likely influences the critical value of A. However, this cannot be confirmed in this study, as the geometry of the vehicle was kept constant across all scenarios.

3.2. Effect of the volume of the flammable mixture

The effect of the variation of the volume of the flammable mixture was studied through parameters B and C. Fig. 5 shows the effect of the gas cloud extension in the horizontal plane (parameter B) on the explosion strength. It can be observed that the effect plateaus after a certain value. The value of B at which this occurs appears to relate to the size of the configuration. In the configuration with 1 × 1 vehicle, B reaches its maximum effect at 0.5 m. Thereafter, the effect remains virtually constant. However, in the configuration with 3 × 3 vehicles, the overpressure continues increasing up to $B = 1.0$ m before stabilising. It is worth noting that A was equal to 0.5 m in all scenarios in Fig. 5. For

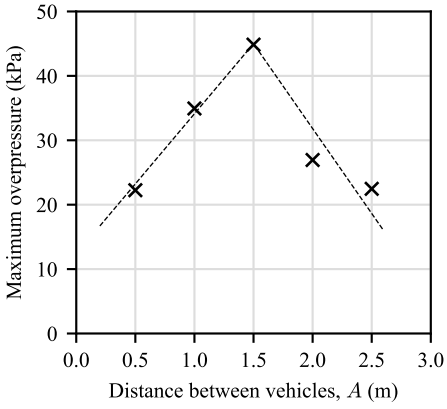

Fig. 4. Maximum overpressure as a function of parameter A. Scenarios I-01 to I-05.
The dashed lines were added based on a visual inspection.

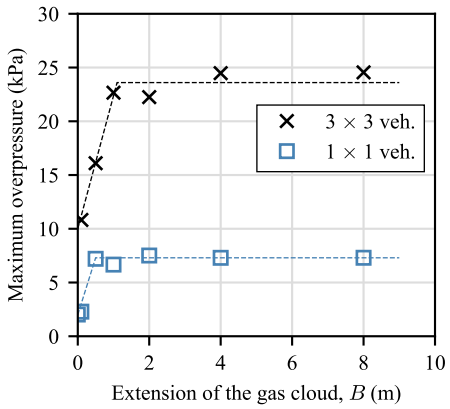

Fig. 5. Maximum overpressure as a function of parameter *B*.
Scenarios I-01, I-06 to I-15, and I-24. The dashed lines were added based on a visual inspection.

greater values of *A*, the maximum effect may occur at greater values of *B*. Indeed, Lozano [41] reported that convergence of the effect of *B* appeared, on average, at about 2 m, based on cross-examination of scenarios with *A* equal to either 0.5, 1.5 or 2.5 m.

A similar effect of parameter *B* on the peak impulse was found. This is evidenced in Fig. 6, which shows the peak impulse profile along a path perpendicular to the main vehicle direction. The path crosses the ignition point. Clearly, the impulse increases with increasing *B*. However, no significant enhancement was achieved for $B > 2.0$ m. It should be noted that the impulse in Fig. 6 was calculated for the initial, major positive phase. However, the secondary (and minor) positive phases in the overpressure-time histories at monitor points displayed greater impulse content in scenarios with greater *B* due to the larger volume of uncongested gas.

The stabilisation of the effect of *B* is attributed to two main reasons. The first relates to continued flame acceleration in the recirculation zone outside the group of vehicles caused by the turbulence downstream of the last vehicle generated by the flow leaving the congested region. This results in greater overpressure outside the configuration. However, flame acceleration only occurs over a limited distance outside the vehicle group before the flame speed starts to decay. No further enhancement of the overpressure occurs when the flame reaches the decaying zone. Thus, if sufficient flammable mixture exits to allow for the full recirculation zone to develop, no significant contribution to pressure enhancement is expected if the volume is increased further. The size of this recirculation zone is expected to depend on the geometry of the configuration, which would explain the dependency between the value at which the effect of *B* levels off, the layout of the vehicles and the separation distance. The second reason is that a greater volume of unburned gas behind the ignition point delays the venting of the combustion products and thus allows for a higher overall flame speed to develop in the confined region under the vehicle group. However, this effect is only significant up to a certain volume of unburned gas outside the configuration.

The effect of the height of the gas cloud (parameter *C*) on maximum overpressure is given in Fig. 7. Like the trend displayed by the effect of *B*, the effect of *C* seems to plateau after a certain value of *C*. In the scenario with 1 × 1 vehicle, the effect levels off at $C = 2.5$ m, while it does so at about $C = 3.0$ m in a scenario with 3 × 3 vehicles. The effect of *C* appears to be less sensitive to the size of the configuration than parameter *B*. A similar trend was observed for the influence of *C* on the peak impulse. The factorial analysis in [41] indicated signs of convergence of the effect of *C* at 2.7 m on average, which lies between the two values observed here.

3.3. Number of vehicles

Fig. 8 shows the maximum overpressure as a function of the number of vehicles in the transverse direction (parameter *D*) and longitudinal direction (parameter *E*). For a given value of *E*, there is an initial, nearly linear relationship between maximum overpressure and parameter *D*. However, the effect of *D* levels off as *D* increases. Indeed, the effect shows a clear plateau for the scenarios with $E \leq 2$. Stabilisation of the effect of *D* emerges earlier for the smaller value of *E*. In the scenarios with $E = 3$, while the effect of *D* continues increasing up to $D = 5$, stabilisation may be expected to occur for some value of *D* greater than five.

The results indicate a strong correlation between the explosion strength and the number of vehicles in the transverse direction. This outcome agrees with the observations in [41]. Lozano [41] argued that the main reason for this is the interaction of the flow with the "long" side of the wheels. That is, flame propagation perpendicularly to the direction of traffic leads to greater overpressure. Furthermore, the results indicate that the effect of *D* on the maximum overpressure may eventually be surpassed by the alleviating effects of side relief in configurations sufficiently elongated in the transverse direction. Puttock [71] reported a similar trend for explosions in long, narrow areas in process plants based on calculations with EXSIM CFD. This behaviour was not observed in [41] as the parametric study in that work was limited to a maximum of three vehicles in either direction. It is worth noting that the effect of *E* appears negligible if the effect of *D* has not yet levelled off. However, *E* clearly plays a role in the value at which the effect of *D* plateaus.

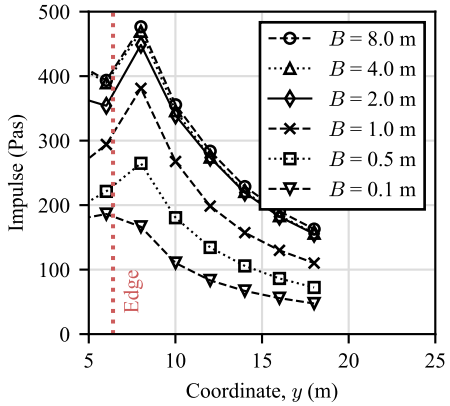

Fig. 6. Impulse as a function of distance and parameter *B*.
Scenarios I-01 and I-11 to I-15. The vertical dotted line gives the edge of the configuration.

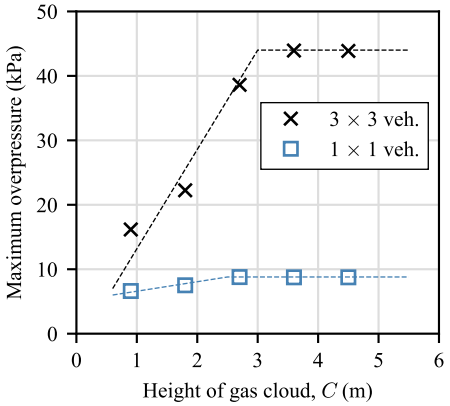

Fig. 7. Maximum overpressure as a function of parameter *C*.
Scenarios I-01 and I-16 to I-24. The dashed lines were added based on a visual inspection.

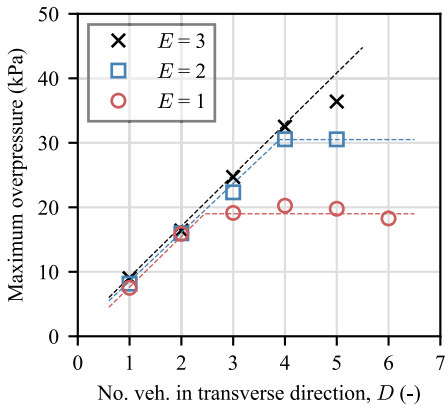

Fig. 8. Maximum overpressure as a function of parameters D and E. Scenarios I-01 and I-24 to I-38. The dashed lines were added based on a visual inspection.

4. Initial formulation of the proposed approach

The results of interest that this study seeks to predict with the MEM are the peak overpressure, ΔP^+, and peak positive impulse, i^+, generated by the VCE. At a given point in the calculation domain, the CFD solver provides the variation of the overpressure over time, $\Delta P(t)$. From this, ΔP^+ and i^+ can be calculated. If the peak overpressure and peak positive impulse at all studied points are assembled in the vector $\boldsymbol{Y} = [\boldsymbol{\Delta P^+}, \boldsymbol{i^+}]$ and the CFD solver is treated as a function $\boldsymbol{F}$, then

$$\boldsymbol{Y} = \boldsymbol{F}(\boldsymbol{X}) \tag{3}$$

The vector $\boldsymbol{X} = \{A, B, C, D, E, \textit{vehicle geometry}\}$ is the set of input parameters defining the studied scenarios. Since running $\boldsymbol{F}$ is resource-intensive, the goal of this research is to calibrate a simplified approach based on the MEM whose approximate $\boldsymbol{Y}^*$ predictions are, from a statistical point-of-view, close to the "true" output $\boldsymbol{Y}$. However, a sufficiently close approximation may not be possible due to the underlying simplifications in the MEM concept. A conservative prediction is desirable in such a case. If the MEM calculations are represented with the function $\boldsymbol{F}^*$, then

$$\boldsymbol{Y}^* = \boldsymbol{F}^*(\boldsymbol{V}, \boldsymbol{S}, \boldsymbol{R}) \tag{4}$$

The vector $\boldsymbol{V}$ contains the volume of the equivalent blast source, which is used for estimating the energy of combustion. The vector $\boldsymbol{S}$ contains the strength class. Finally, the vector $\boldsymbol{R}$ contains the stand-off distances to the studied points. Thus, the goal of the study is to provide guidelines for determining $\boldsymbol{V}$, $\boldsymbol{S}$, and $\boldsymbol{R}$ based on the defining parameters of the scenario of interest. This chapter introduces the initial formulation of the approach, including a strategy for considering the directional blast effects due to asymmetry in the scenario. It is assumed that the total volume of available flammable material is significantly greater than the volume of the congested region. The approach is validated in Section 5, with modifications incorporated where necessary.

4.1. Size of the equivalent blast source

The MEM approximates the explosion energy as the product of the specific heat of combustion and the volume of the equivalent blast source. The specific heat of combustion is assumed to be equal to 3.5 MJ/m^3, regardless of the mixture composition. Thus, estimating the explosion energy is reduced to estimating the volume of gas at the source of a strong blast, V_{source}.

For the scenarios of interest, the blast source is represented by a fuel-air cloud of cuboid shape. This gas cloud should extend beyond the edge of the group of vehicles in all directions to account for flame acceleration outside the congested region. If the vehicles are arranged in a regular configuration, the dimensions of the blast source are given by Eqs. (5)–(7). The total volume of the equivalent source is then defined by Eq. (8). The parameters l_{car}, b_{car}, h_{car}, and V_{car} are the length, width, height (including the wheels) and volume of one vehicle. Evidently, the dimensions of the blast source depend on the number of vehicles (parameters D and E) and the separation distance between vehicles (parameter A). These parameters are readily available for a given scenario or can be easily evaluated based on the layout of the road or carpark and the traffic conditions. Therefore, the challenge in calculating V_{source} lies in the estimation of its extension outside the congested region: e_x, e_y and e_z.

$$l_{source} = E \cdot l_{car} + (E-1) \cdot A + 2 \cdot e_x \tag{5}$$

$$b_{source} = D \cdot b_{car} + (D-1) \cdot A + 2 \cdot e_y \tag{6}$$

$$h_{source} = h_{car} + e_z \tag{7}$$

$$V_{source} = l_{source} \cdot b_{source} \cdot h_{source} - D \cdot E \cdot V_{car} \tag{8}$$

The values at which the effects of B and C on the maximum overpressure level off can be conveniently used for a preliminary definition of e_x, e_y and e_z. The values at which the effects of B and C stabilise appeared to change with the size of the configuration. However, it is desirable to find values that provide acceptable prediction for any number of vehicles, so that e_x, e_y and e_z could be treated as constant in Eqs. (5)–(7). Based on the results presented in Section 3.2 and those reported in [41], we propose to assume that all the gas volume within $B = 2.0$ m and $C = 2.5$ m is part of the source of strong blast. That is, $e_x = e_y = B = 2.0$ m and $e_z = C - h_{car} = 1.0$ m.

Notably, other authors have recommended extending the gas volume 2.0 m beyond the congested region [71,72], although such recommendations were intended for settings within process plants, in which obstacles are of smaller scale than the vehicles discussed here. Moreover, those recommendations were also to be applied in the vertical direction, which would result in a cloud height of 3.5 m for the scenarios in this article. Such a large height is not considered necessary for the scenarios here, given the behaviour of the effect of parameter C. Pitblado et al. [55] recommended using a cloud height of 1.8 m for carparks, meaning that the chosen value of 2.5 m lies between the values given by other authors.

4.2. Directional blast effects

The standard MEM assumes point symmetry of the blast source and blast wave propagation. This assumption is questionable in the near field, where the non-symmetry of the obstructed region introduces a strong directionality to the combustion process [54,73]. Indeed, the scenarios analysed in this study showed significant directional blast loads, particularly in the vicinity of the vehicle group. Thus, a modification should be introduced to improve the MEM accuracy for near-field applications.

In the analysed scenarios, the greatest overpressure values were obtained in localised areas outside the congested region, on the side opposite the ignition point. The results suggest that these localised areas of high overpressure may be treated as separate, external explosions of greater strength (in terms of overpressure) but with lower energy content. The remaining gas volume in the source could then be treated as a global explosion of lower strength but greater energy. Therefore, the approach in this article distinguishes between a localised external source with volume V_{lc} (subscript $_{lc}$) and a global source with volume V_{gl} (subscript $_{gl}$). The sum of these two volumes equals V_{source}.

Combustion in the recirculation zone in the wake of the vehicles is considered the main driving factor of the external localised explosion. Thus, it is reasonable to estimate V_{lc} (and thus the energy contributing to the localised explosion) based on a certain gas volume outside the group of vehicles. The size of the recirculation zone relates to the velocity of

the flow (and corresponding turbulent vortices) exiting the configuration; this, in turn, is connected to the size of the configuration. However, we propose considering the effects of the configuration size only when choosing the strength class while keeping the external volume calculation as simple as possible. In that sense, it is desirable to assume a constant volume for the localised source that works for any number of vehicles.

The definition of the gas outside the congested region has previously been set to $e_x = e_y = 2.0$ m. This definition implicitly considers the size of the recirculation zone. Thus, it is natural to let the localised source have the same width. The other dimensions are taken as the projection of a single vehicle. For a path perpendicular to the vehicle, the volume V_{lc} is given by Eq. (9). The location of the localised source is shifted as the angle of the evaluated path changes, as shown in Fig. 9. However, for the sake of simplicity, the volume of the localised source related to a perpendicular path (given by Eq. (9)) is used for all other angles.

$$V_{lc} = (2.0\,\text{m}) \cdot l_{car} \cdot h_{car} \tag{9}$$

Finally, the gas volume contributing to the global explosion, V_{gl}, is calculated as the difference between the total gas volume and the volume of the localised source, as given by Eq. (10).

$$V_{gl} = V_{source} - V_{lc} \tag{10}$$

In summary, the vector $\boldsymbol{V}$ contains the volume of gas contributing to the blast generation at the global and local sources. If there is sufficient flammable material, this vector is a function solely of the geometry of the congested region and can be formally defined as:

$$\boldsymbol{V} = \{V_{gl}, V_{lc}\} \tag{11}$$

The distinction between localised and global explosion implies that, at a given point, two different stand-off distances must be calculated. The distance from the global source, R_{gl}, is measured from the centre of the configuration. The distance from the localised source, R_{lc}, is measured from the edge of the vehicle group along a straight line connecting the centre of the configuration to the studied point, as shown in Fig. 9. Thus, the vector $\boldsymbol{R}$ contains the stand-off distances from the centres of the respective explosions to the studied points and is formally defined as:

$$\boldsymbol{R} = \{\boldsymbol{R}_{gl}, \boldsymbol{R}_{lc}\} \tag{12}$$

4.3. Choice of strength class

The parametric study showed that the number of vehicles in the transverse direction (parameter D) is the most prominent factor relating to the resulting overpressure. Therefore, it is reasonable to relate the strength class of an explosion scenario consisting of a group of vehicles to parameter D. Moreover, the influence of parameters A, B, and C could be maximised to achieve a conservative prediction. However, the number of vehicles in the longitudinal direction, E, was found to have an important effect in configurations with high D/E ratio and needs to be accounted for when estimating the explosion strength.

Both the localised and the global explosion are associated with a given strength class, which needs to be determined separately. It is assumed that the strength of both explosions can be based primarily on the number of vehicles, D. However, depending on E, correction of the strength class may be needed for elongated configurations. The vector $\boldsymbol{S}$ contains the strength class of the global and localised explosions, S_{gl} and S_{lc}, respectively, as defined by Eq. (13).

$$\boldsymbol{S} = \{S_{gl}, S_{lc}\} \tag{13}$$

Due to the desire to maximise the influence of parameters A, B, and C, it was not possible to determine the relationship between the number of vehicles and the strength class based on the scenarios included in the parametric study. Thus, a new set of reference scenarios was created for the initial fitting of the strength class. These are scenarios II-01 to II-05 in Table B.2. These reference scenarios were defined by $A = 1.5$ m, $B = 4.0$ m, $C = 3.6$ m, $E = 3$, while D was varied between 1 and 5. Note that parameters B and C were set large enough to be beyond the value at which their effects level off. The ignition point was placed at the longitudinal edge of the configuration.

The estimation of the strength class for the localised explosion was based on the maximum overpressure obtained with CFD calculations for each scenario. The maximum overpressure was averaged over a volume of 1 m^3 around the peak value to smooth out the localised peaks. The maximum overpressure for each scenario is presented in Fig. 10. As expected, a strong effect of D is observable: an increase in D results in a greater overpressure. There appears to be an exponential relationship between D and the maximum overpressure. In that sense, the results in Fig. 10 differ from the results in Fig. 8, in which a nearly linear relationship was observed before the effect of D stabilised. This may be due to the influence of the other parameters (A, B and C), whose effect was maximised in the reference scenarios.

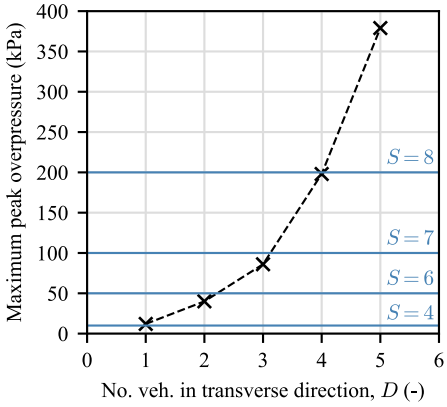

Fig. 10. Relationship between parameter D and the maximum peak overpressure in the reference scenarios.

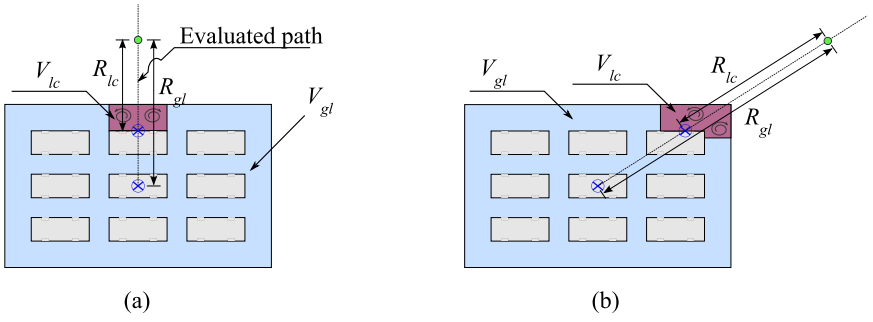

Fig. 9. Schematic representation of the localised source: (a) Evaluated path perpendicular to the main direction; (b) Evaluated path at 45°.

Fig. 10 gives the closest strength class in the MEM for scenarios with $D \leq 4$. For these scenarios, the choice of strength class was relatively straightforward. However, for $D = 5$, the maximum peak overpressure (379 kPa) lies between classes 8 (200 kPa) and 9 (500 kPa), with a significant step in between. A strength class of 9 was chosen, as conservative results are prioritised. However, overprediction is expected in this case.

The blast load arising from the global explosion dominates in the far field. Thus, the calibration of the strength class of the global explosion was achieved by comparing the profiles of overpressure versus distance obtained with CFD calculations and the MEM. With this procedure (unlike the strength class for the localised explosion), the strength class for the global explosion is affected by the choice of the gas volume at the source. That is, the determined strength class numbers are valid only if the guidelines for calculating the volume of the source are followed. Table 2 shows the calculated gas volume for the global and localised explosions, according to the procedure for implementing the MEM outlined in Sections 4.1 and 4.2.

At a given point, the peak overpressure due to the localised explosion, ΔP^+_{lc}, and the global explosion, ΔP^+_{gl}, were determined separately for different strength classes. Thereafter, the dominant peak overpressure, ΔP^+_{MEM}, was calculated using Eq. (14). This calculation was conducted at all cell centres in the core domain outside the congested region.

$$\Delta P^+_{MEM} = \max\left(\Delta P^+_{lc}, \Delta P^+_{gl}\right) \tag{14}$$

Two metrics were used to determine the most suitable strength class for the global explosion. First, the mean value absolute error (MAPE) was used to evaluate the overall performance of a given strength class. The MAPE was calculated using Eq. (15), in which n is the number of points evaluated and ΔP^+_{CFD} is the corresponding peak overpressure from the CFD simulations. However, the mean bias was limited to $MG_p > 0.7$ to avoid excessively underpredicting the overpressure. Furthermore, as the goal was to calibrate the global explosion, the only results considered were at points outside the localised explosion's main area of influence. The most suitable strength of the global source was then identified iteratively for all reference scenarios.

$$\text{MAPE} = \frac{1}{n}\sum_{1}^{n}\left|\frac{\Delta P^+_{CFD} - \Delta P^+_{MEM}}{\Delta P^+_{CFD}}\right| \tag{15}$$

The determined strength class numbers are given in Table 3. It should be emphasised that this calibration was made regarding the peak overpressure. The following section will verify the performance of the peak impulse prediction using the MEM with these strength class numbers.

Table 2
Estimated volume of the equivalent blast source in the reference scenarios.

Scenario ($D \times E$)	V_{source} (m^3)	V_{gl} (m^3)	V_{lc} (m^3)
1 × 3	279	265	14
2 × 3	424	410	14
3 × 3	569	555	14
4 × 3	714	700	14
5 × 3	859	845	14

Table 3
Initial recommendations of strength class for the localised and global explosion.

D (-)	S_{lc} (-)	S_{gl} (-)
1	4	4
2	6	5
3	7	6
4	8	7
5	9	8
≥ 6	≥ 9	≥ 8

5. Validation and additional considerations

This chapter presents the comparison between the prediction with the MEM following the approach formulated in Section 4 and the corresponding results from CFD simulations. Initially, the prediction was verified for the five reference scenarios introduced in Section 4.3. Thereafter, additional scenarios were studied to evaluate and adjust the MEM approach for long and narrow configurations. Finally, a methodology was introduced to account for the fuel type. The additional scenarios studied in this section are described in Table B.2. The label of the scenarios in all plots follows the rule $D \times E$.

5.1. Prediction of overpressure in the reference scenarios

Fig. 11 shows the calculated peak overpressure as a function of the energy-scaled distance, using both the proposed approach with the MEM and CFD calculations for two selected scenarios. The asymmetry and directionality of the overpressure become evident by the spread of the CFD results at a given distance (blue data). In a completely point-

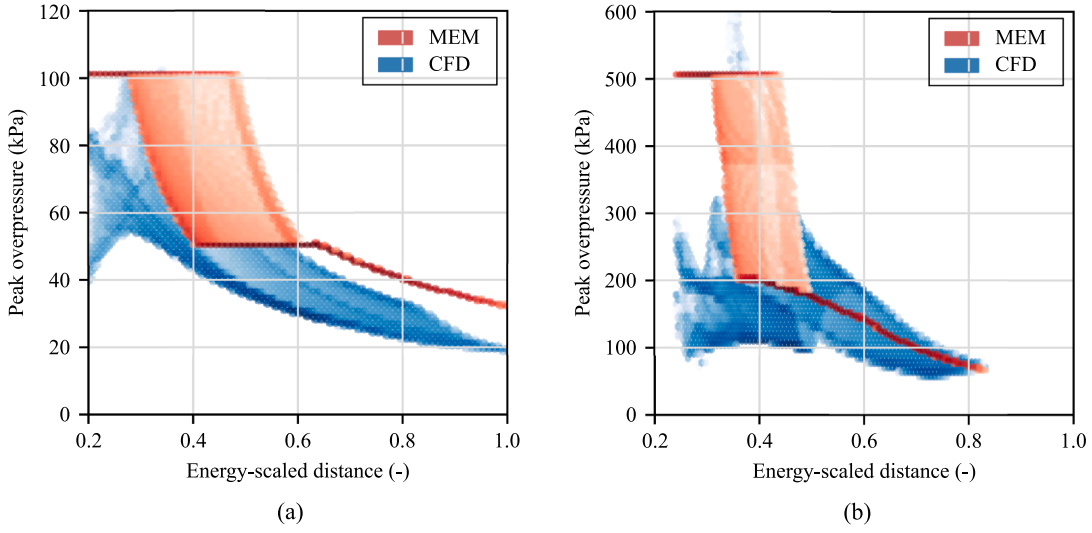

Fig. 11. Comparison of peak overpressure in two of the reference scenarios: (a) Results for the scenario with 3 × 3 vehicles; (b) Results for the scenario with 5 × 3 vehicles. The distance was scaled with regard to V_{source}.

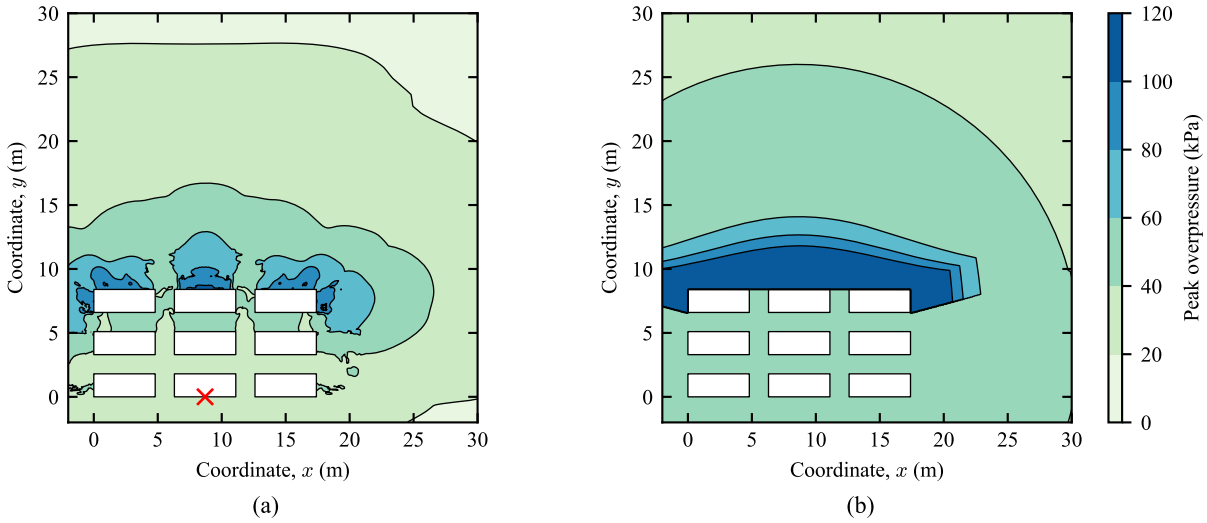

Fig. 12. Comparison of contour plots of peak overpressure for the 3 × 3 scenario: (a) CFD calculations; (b) Prediction with the MEM. The red cross represents the ignition point in the CFD model.

symmetrical explosion, the results would lie upon a curve. The localised source in the MEM, whose centre is assumed to vary with the position of the studied point, is intended to account for such directional blast effects. Indeed, its contribution also appears as a wide band in the figure. Further away from the congested region, where the global explosion (whose centre remains fixed) prevails over the localised source, the MEM prediction assumes the shape of a curve, indicating a hemispherical expansion of the blast wave. In all scenarios, the global explosion governs the prediction at energy-scaled distances greater than 0.6.

Among all reference scenarios, the cases presented in Fig. 11 have the poorest performance indicators concerning overpressure prediction (MG_p and VG_p). For the 3 × 3 scenario, $MG_p = 1.45$ (which exceeds the desired target: MG < 1.3) and $VG_p = 1.17$ (which fulfils the desired target: VG < 1.6). Indeed, the global explosion in the MEM (which dictates the position of the "tail") overpredicts the overpressure compared to the CFD results, as given in Fig. 11(a). However, using the strength class immediately below would have resulted in significant underprediction, violating the criterion $MG_p > 0.7$. In the 5 × 3 scenario, the position of the "tail" is close to the mean value of the CFD results, but significant deviations are still visible close to the explosion centre, as shown in Fig. 11(b). For this scenario, $MG_p = 1.45$ and $VG_p = 1.44$. Nevertheless, if only the tail of the prediction is considered, then $MG_p = 1.12$ and $VG_p = 1.09$.

Figs. 12 and 13 give the contour plot of peak overpressure for two scenarios based on CFD analysis and the MEM approach. These figures show that the localised explosion is only relevant on the side of the configuration opposite the ignition point. Moreover, comparison across different scenarios showed that the contribution of the localised source in the calculations with the MEM need only be considered within a circle segment of 150° with its origin at the centre of the configuration, as given in Fig. C.1(c).

Fig. 14 summarises the comparison of calculated values of peak overpressure with the MEM and CFD analyses for the five reference scenarios. The results are presented as hexagonal binning plots, in which a darker shade implies a greater concentration of data points. The black diagonal line represents an ideal correlation between the MEM and CFD analyses, whereas the dashed red lines correspond to ±30 % deviation from the perfect correlation. The MEM can be seen to overpredict the peak overpressure beyond the sought-after limit of +30 % at several zones in the scenarios. Indeed, for scenarios with up to 3 × 3 vehicles,

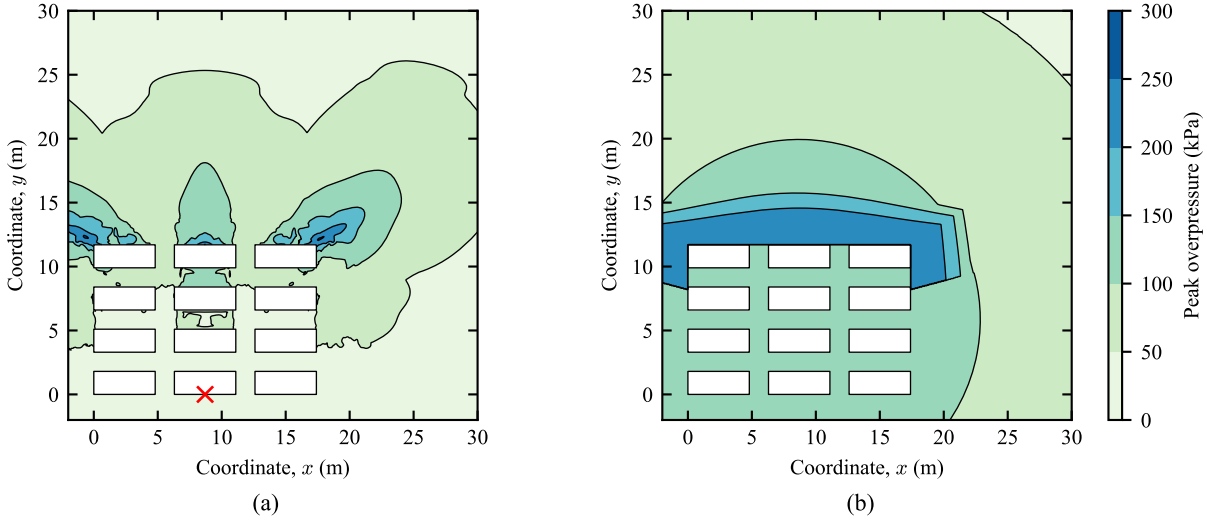

Fig. 13. Comparison of contour plots of peak overpressure for the 4 × 3 scenario: (a) CFD calculations; (b) Prediction with the MEM. The red cross represents the ignition point in the CFD model.

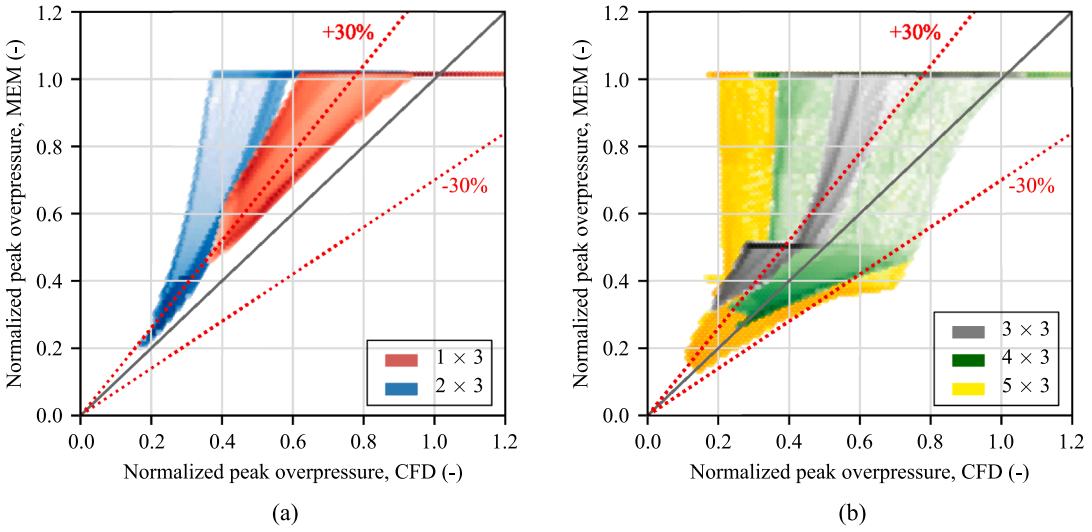

Fig. 14. Comparison of peak overpressure prediction in the reference scenarios.

most of the results lie above the +30 % line (cf. Fig. 11(a)). However, for the scenarios with 4 × 3 and 5 × 3 vehicles (cf. Fig. 11(b)), a significant portion of the data set is within the intended error margin.

There are different reasons for overestimating the peak overpressure with the MEM. One significant reason is that, in some cases, the step between strength classes in the MEM is too great. If the next lowest strength class were to be applied, the MEM would instead underpredict the overpressure and to a greater extent than the current overprediction. Another important phenomenon is that the localised areas with high overpressure values become comparably smaller as the explosion strength increases. Furthermore, the difference between overpressure in the localised areas and in the zones between them increases with greater maximum overpressure. This becomes evident when comparing the results in Fig. 11 and the contour plots of maximum overpressure in Figs. 12 and 13. In contrast, the MEM approach "sweeps" along the entire edge of the configuration. Consequently, the prediction in the zones between localised areas will overpredict the peak overpressure. This is why the left edges of the binning plots in Fig. 14 appear to become more vertical as the configuration grows. Note that changes in the layout of the configuration and the position of the ignition point affect the distribution of the localised zones. Due to this uncertainty, it is reasonable to assume that the entire edge opposite the ignition point acts as a localised source in the MEM.

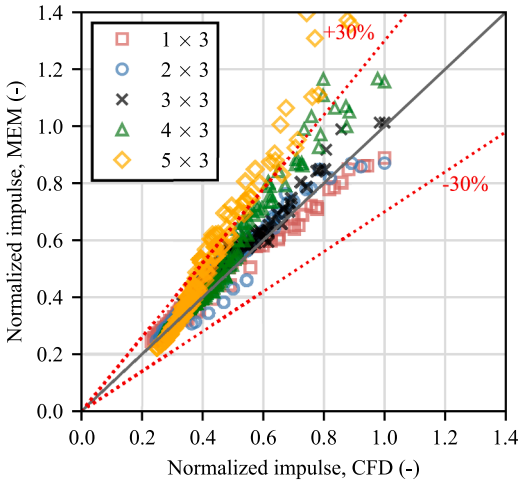

Fig. 15. Comparison of peak impulse prediction in the reference scenarios.

5.2. Prediction of impulse in the reference scenarios

The peak impulse values calculated using the MEM and CFD analysis are compared in Fig. 15 at multiple monitor points. The total impulse at a given point according to the MEM was calculated using Eq. (16), in which i_{lc}^{+} is the peak impulse due to the localised explosion and i_{gl}^{+} is the peak impulse due to the global explosion. The results are normalised with regard to the greatest impulse value from the CFD results. Good agreement was obtained for the studied scenarios. In general, the scatter seems to be greater for points located close to the explosion centre, while the prediction improves at a greater distance. The MEM prediction was very good for the scenarios with up to 3 × 3 vehicles. Indeed, all data points for these scenarios lie between the ±30 % interval and are well distributed around the ideal correlation. For these scenarios, the performance indicators concerning impulse prediction display $MG_i < 1.08$ and $VG_i < 1.01$. For the scenario with 4 × 3 vehicles, a few points are located about the +30 % limit. For the 5 × 3 scenario, several result points exceed the desired target of +30 %. Despite this, this scenario displays $MG_i = 1.16$ and $VG_i = 1.05$ if all points are considered. However, MG_i would exceed 1.3 if points in the vicinity of the configuration were the only ones being considered.

$$i_{MEM}^{+} = i_{lc}^{+} + i_{gl}^{+} \tag{16}$$

Fig. 16 shows the calculated peak impulse as a function of the energy-scaled distance. The scattered points are the results of the CFD analyses. The continuous lines give the average predicted peak impulse from the MEM. The figure shows that the MEM overpredicts the peak impulse in the near field for scenarios 4 × 3 and 5 × 3. However, the prediction for scenario 4 × 3 is still within the accepted range at most points, as shown in Fig. 15.

The main reason for the larger error for stronger explosions is the initial assumption of triangular overpressure-time history for all strength classes. While this assumption provides satisfactory results for the weaker explosions, it introduces a prediction error for the strongest ones. This error appears to become critical for $S \geq 8$. To test the performance of a different blast waveform, an analogy is drawn between the strongest explosions and a high explosive detonation. That is, the overpressure-time curve for these explosions is assumed to follow the Friedlander waveform[4]. Under this assumption, the impulse obtained is

[4] The Friedlander waveform is commonly used for blast waves generated by detonation of high explosives.

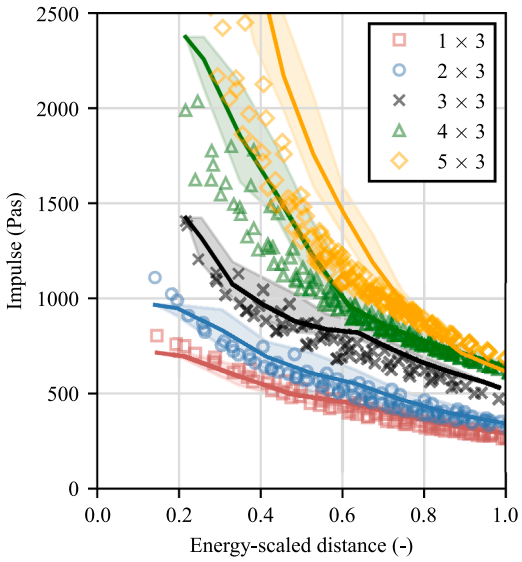

Fig. 16. Peak impulse prediction as a function of the energy-scaled distance in the reference scenarios.
The scattered points are the results of the CFD analysis. The lines represent the MEM prediction, while the shaded area gives its predicted scatter. The distance was scaled with regard to V_{source}.

around 74 % of that with a triangular waveform having the same peak overpressure and duration. Fig. 17 shows the comparison if the Friedlander waveform is used for strength class $S \geq 8$. Much better agreement was obtained for the 4 × 3 and 5 × 3 scenarios, with only a handful of data points outside the accepted range.

In general, the peak impulse prediction was found to be less sensitive to the configuration asymmetry. One likely reason for this is that the impulse content of the highest overpressure peaks is relatively small compared to the overall impulse content of the wave. Indeed, in the near field, the contribution of the localised source to the total impulse was around 30 % at most. Further away from the explosion, the influence of the localised source diminishes (around < 10 %). Hence, for points placed further away, a good approximation could be achieved by considering solely the global explosion. This holds for all scenarios for an energy-scaled distance greater than 0.6.

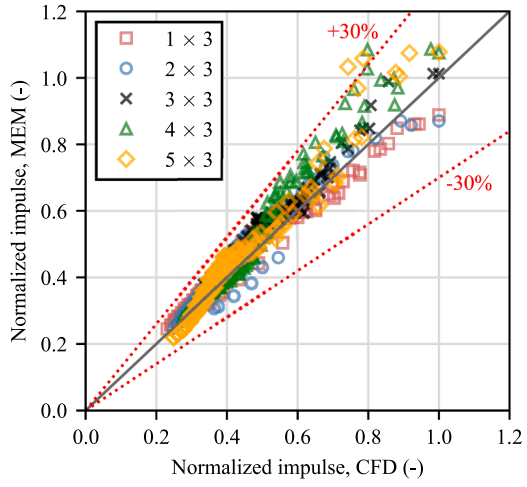

Fig. 17. Comparison of peak impulse prediction in the reference scenarios, assuming Friedlander waveform for $S \geq 8$.

5.3. Configurations elongated in the transverse direction

The initial fitting of the strength class in the MEM was conducted on scenarios that fulfilled $D \leq 5$ and $E = 3$. However, previous analyses have indicated that side venting limits pressure build-up for an increasing ratio of D/E. These are configurations that are long and narrow in the transverse direction. Thus, the previously determined strength class is likely to overestimate the explosion pressure for configurations characterised by a high D/E ratio.

This section investigates the performance of the MEM in configurations elongated in the transverse direction. Two groups of scenarios were studied. In the first, parameter E was fixed at 1 while D was varied (Scenarios II-06 to II-09 in Table B.2). In the second, factor E was set to 2 (Scenarios II-10 to II-13 in Table B.2).

Fig. 18(a) shows the comparison of peak impulse between the CFD analyses and MEM calculations for the scenarios with $E = 1$. There was good agreement between MEM and CFD for the $D \leq 3$ scenarios. However, in the $D > 3$ scenarios, the MEM overpredicted the peak impulse in the near field. Indeed, several result points for the two larger scenarios lie outside the +30 % margin. Fig. 18(b) shows the comparison of the cases in the second group, for which $E = 2$. Likewise, there is very good correspondence for the scenarios with $D \leq 3$. For the $D > 3$ scenarios, there was overprediction in the near field, though less than in the corresponding scenarios in the $E = 1$ group. This demonstrates that the initial choice of strength class based solely on $E = 3$ scenarios (particularly the strength class of the localised explosion) may be overly conservative for elongated, transverse configurations. There was a similar trend for the prediction of peak overpressure.

A lower strength class should therefore be used in elongated, transverse configurations. The corrected strength class numbers for these scenarios are given in Table 4. The recommended approach to estimating the size of the equivalent blast source in these configurations remains unchanged. Fig. 19 shows the peak impulse prediction comparison with the corrected strength classes. Clearly, the prediction improved significantly. For these scenarios, the performance indicators lie within $0.85 < MG_i < 1.07$ and $VG_i < 1.03$. The prediction of peak overpressure also improved with the reduced strength class. However, scenario 4 × 1 displayed a large mean bias value, $MG_p = 1.73$. Although above the sought-after target of 1.3, this indicator is still within a factor of two from the mean, which is a commonly accepted upper limit. This, coupled with the very good peak impulse prediction, indicates adequate overall results, even for this scenario.

5.4. Configurations elongated in the direction of traffic

Flame propagation in the transverse direction (which relates to parameter D) has been found to enhance pressure build-up. Thus, the strength class so far determined is primarily suitable in those zones where the flame moves perpendicularly or at a significant angle from the direction of traffic. In configurations elongated in the direction of traffic, as the flame travels down the line of vehicles away from the ignition point, the general direction of the flame becomes predominantly parallel to the main direction of the vehicles. In these zones, the combustion process is likely to be characterised by a lower strength class. This gains relevance as parameter E increases in relation to D (a low D/E ratio). In such configurations, it is therefore necessary to determine what size of blast source should be assumed when using the proposed strength classes.

To evaluate this aspect, two groups of scenarios were studied. The first consisted of cases with $D = 2$ and variable E (Scenarios II-02, II-10 and II-14 to II-16), while the cases in the second group had $D = 3$ and variable E (Scenarios II-03, II-11, II-17 and II-18).

It was found that the maximum overpressure in the studied scenarios was not significantly affected by the value of E. However, the length of the configuration had a discernibly clear effect on the peak impulse. In general, the magnitude of the peak impulse at a given distance was

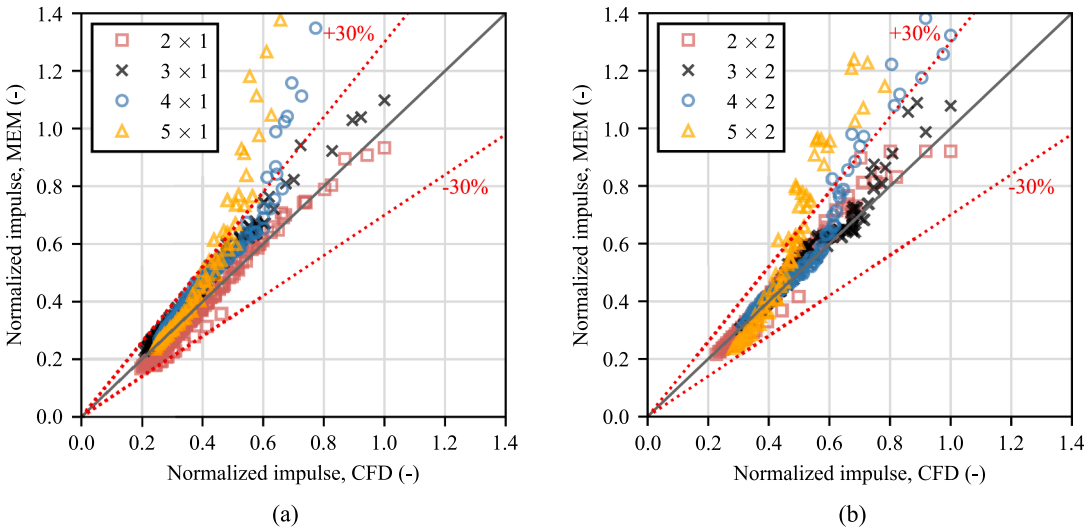

Fig. 18. Comparison of peak impulse prediction in elongated, transverse configurations.

Table 4
Corrected strength class for elongated, transverse configurations.

D (-)	$E = 1$		$E = 2$	
	S_{lc} (-)	S_{gl} (-)	S_{lc} (-)	S_{gl} (-)
3	7	5	7	6
4	7	6	7	7
5	7	6	8	7

lowest for the scenarios with $E = 1$ and it increased as the value of E increased. However, no significant increase was observed for $E > 3$. This indicates that the size of the equivalent source does not continue increasing after a certain value of E. This trend was more significant in scenarios with $D = 2$.

These results suggest that there is a maximum gas volume that contributes to strong blast generation for a given number of vehicles in the transverse direction, while combustion in the adjacent areas will be of lower strength. Therefore, when using the MEM, the effective length of the source of the blast should be limited to an upper value $l_{source.max}$, as depicted schematically in Fig. 20. A comparison between CFD and MEM predictions showed that setting $l_{source.max} = 2.5 \bullet b_{source}$ provides good results. In practice, this means that for very long traffic queues, not all vehicles would contribute to the strongest explosion to the same degree. That is, if the length of the line of vehicles exceeds $l_{source.max}$, the explosion characteristics at a point perpendicular to the position of the ignition point would be similar, regardless of the number of vehicles in the longitudinal direction.

Fig. 21 presents the prediction of impulse with the MEM for the studied configurations imposing $l_{source.max}$. In general, there is very good agreement and the scattered points seem to overlap across the same regions, regardless of E. For these scenarios, the performance indicators show $0.96 < MG_i < 1.09$ and $VG_i < 1.02$.

5.5. General evaluation of the statistical performance indicators

Fig. 22 shows the plot of geometric variance (VG) versus geometric mean (MG) when predicting peak overpressure and peak impulse for all studied scenarios. Where relevant, the reduced strength class numbers according to Section 5.3 were used, plus the limitation on the mobilised gas volume introduced in Section 5.4. The shaded region represents a region in which the criteria for a "good" model are met: $0.7 < MG < 1.3$ and $VG < 1.6$. The vertical, dark, dashed line represents no systemic bias. Points placed to the right of this line indicate overestimation by the MEM with respect to the CFD analysis, while points to the left indicate

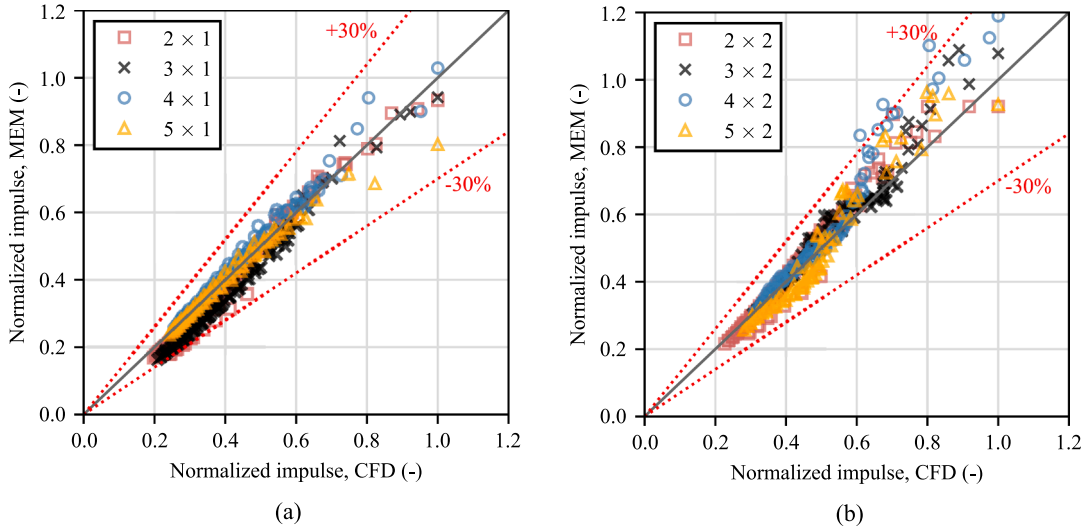

Fig. 19. Comparison of peak impulse prediction with reduced strength class in elongated, transverse configurations.

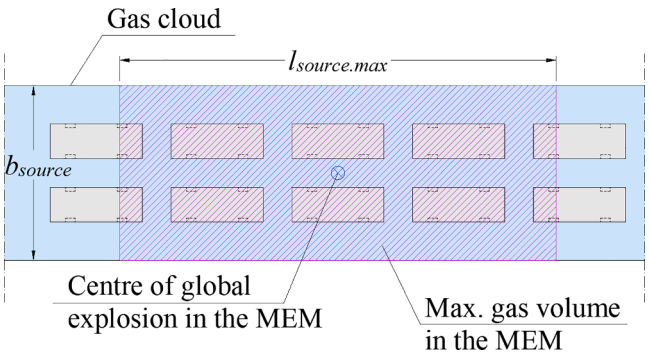

Fig. 20. Schematic definition of the maximum length of the equivalent blast source.

underestimation. The solid black parabola indicates the minimum possible variance for a given geometric mean. Points lying on or close to this line show systematic bias without significant scatter.

Regarding the prediction of peak overpressure, noticeable overprediction was obtained for most scenarios. In contrast, only one scenario showed minor underprediction. The greatest overprediction was obtained for the scenario with 4 × 1 vehicles. As explained before, if an accurate prediction of overpressure with the MEM was not possible at all zones of the scenarios, then overprediction was to be preferred. Overprediction stems mainly from the limitation of there being only 10 strength classes in the MEM, a high degree of directionality of the blast load, and a strong variation of overpressure between the localised patches of high overpressure and their adjacent areas. Nonetheless, all scenarios fulfilled $VG_p < 1.6$, indicating that the introduction of a localised source in the MEM was an effective strategy to minimise the error introduced by the directional blast effects.

All the performance indicators regarding the peak impulse prediction lie inside the approved region, which indicates the good performance of the MEM with respect to the CFD models. The greatest overprediction bias was obtained for the 5 × 3 scenario. The peak impulse was underpredicted for four scenarios, with the 3 × 1 scenario displaying the largest underprediction. Apart from the two extreme cases, the indicators for impulse prediction fulfilled $0.92 < MG_i < 1.08$ and $VG_i < 1.02$. In general, impulse prediction appears less sensitive to the inherent asymmetry of the explosion, which makes the MEM more suitable for predicting this blast wave parameter.

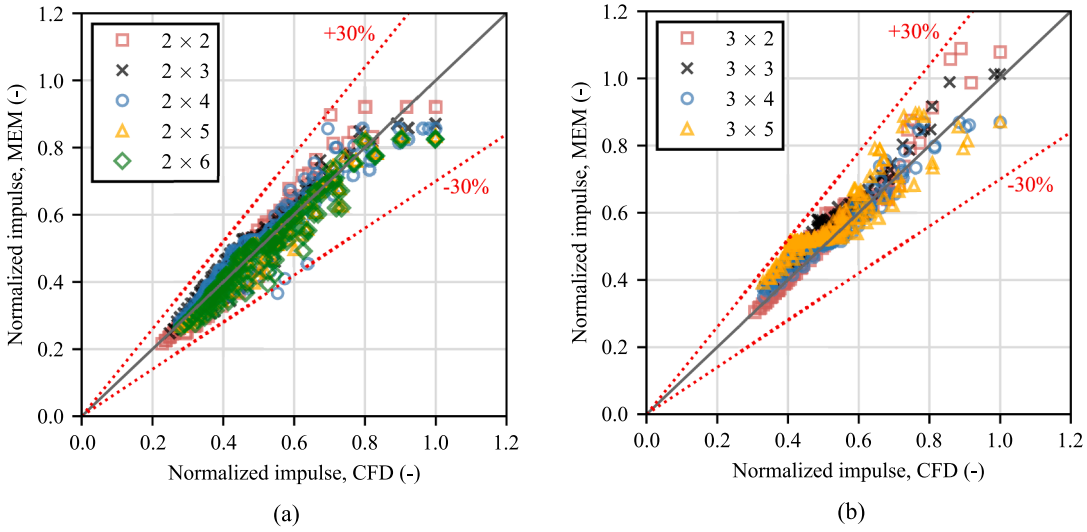

Fig. 21. Comparison of peak impulse imposing $l_{source.max}$ in configurations elongated in the direction of traffic.

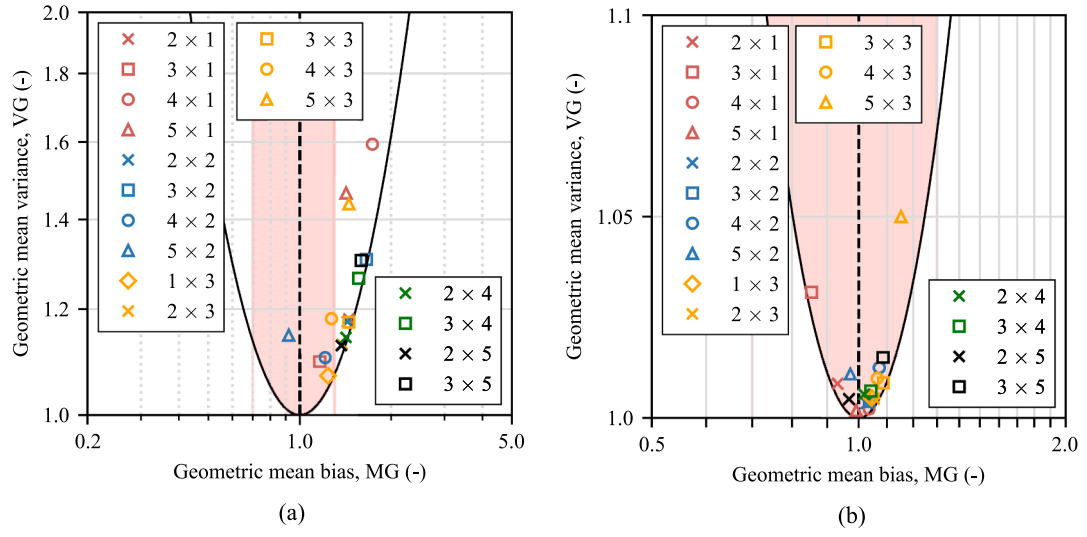

Fig. 22. Performance indicators for prediction of: (a) peak overpressure; (b) peak impulse. The shaded area gives the approved range.

It is worth highlighting that the acceptance criteria used by the CFD software developers (MG < 2, VG < 4) are more lenient than the ones adopted here. Indeed, the indicators of all the studied scenarios are within the accepted range for the software. That is, the results with the modified MEM are, at the very least, within the confidence interval of the CFD code that was used.

5.6. Fuel scaling

Experimental research has shown that the process of turbulent combustion and pressure build-up in gas explosions is significantly affected by the reactivity of the fuel [74,75]. Up to this point, the numerical simulations conducted in this article have assumed mixtures of propane and air. However, lower overpressure and impulse values are expected for otherwise identical scenarios but with a less reactive gas, such as methane. Conversely, greater values are expected with more reactive gases, such as ethylene.

An often-cited scaling theory for considering the effect of fuel reactivity was initially proposed by Taylor and Hirst [76]. Their theory states that the ultimate flame speed is proportional to the product of the laminar burning speed, U_0, and the expansion ratio of the fuel-air mixture, α, raised to the power of 1.36. Further, the theory assumes a quadratic relationship between the maximum overpressure and the flame speed, which results in:

$$P \propto (U_0 \cdot \alpha)^{2.72} \tag{17}$$

Puttock [71] corrected this expression to consider that one unit of volume of gas is consumed as α units of volume are produced, which gives:

$$P \propto [(U_0 \cdot (\alpha - 1)]^{2.72} \tag{18}$$

Based on Eq. (18), the overpressure obtained for a mixture of propane and air could be scaled to other hydrocarbon fuels by multiplying with the correction factor κ, determined as:

$$\kappa = \left[\frac{U_0 \cdot (\alpha - 1)}{U_{0.ref}(\alpha_{ref} - 1)}\right]^{2.72} \tag{19}$$

In which $U_{0.ref}$ and α_{ref} are the laminar burning velocity and the expansion ratio of the reference mixture of propane and air. For the propane-air mixture assumed in this work, the value $U_{0.ref}$ is set to 0.464 m/s (a value used by the CFD code), while α_{ref} is set to 8.09 [77]. Fuel scaling is more suitable for low-to-medium flame speed and is expected to provide acceptable results for $S \leq 8$.

Regrettably, investigation of fuel scaling has focused on the effects on flame speed and overpressure and, to the current knowledge of the authors, no information about impulse scaling exists in the literature. For simplicity, the same factor derived for overpressure can be used for impulse.

This approach was tested for methane-air mixtures in the five reference scenarios introduced in Section 4.3. CFD analyses of these scenarios were conducted using the same approach described in Section 2.3. The only difference was the mixture, which was assumed to be a mixture of methane and air (Scenarios II-19 to II-23). The parameters U_0 and α for the methane-air mixture are equal to 0.448 m/s (a value used by the CFD code) and 7.52 [77]. This gives a correction factor $\kappa = 0.72$. Fig. 23 shows the comparison between CFD results and predictions with the MEM corrected with the calculated factor κ. There was generally good correspondence, although overprediction of the impulse in the near field was obtained for scenarios 4 × 3 and 5 × 3. These results can be compared to the results obtained for a propane-air mixture in Fig. 15. A similar trend can be observed for the two different mixture compositions. All in all, the correction factor appears to provide acceptable results for methane-air mixtures.

6. Discussion

This study investigates the applicability of the MEM for explosion scenarios in traffic environments such as roads and carparks. Supported by CFD calculations, the study produced a set of guidelines for implementing the MEM in these scenarios. These guidelines are summarised in Appendix C. The overall goal was to develop a consistent strategy for estimating the blast load that may affect structures near roads on which the transport of flammable gases is permitted. The results of interest were the peak overpressure and the impulse content of the positive phase. The proposed approach contributes towards minimising the disparity and uncertainties that currently affect the application of MEM in this type of environment.

The recommended approach relates the explosion strength to the number of vehicles in the transverse direction (parameter D). The implication of this is that the number of lanes on the road has a much more significant effect on the resulting load than the length of the queue of vehicles. Likewise, cars parked side-by-side represent a greater risk than cars parked parallel to the street.

The guidance presents predefined tables for reading the strength class based on the layout of the group of vehicles. Since the purpose was to find the class number that best represents the scenarios, the authors believe that this semi-qualitative strategy is adequate. Nonetheless, it differs from other recent methods that provide equations for calculating the explosion strength in settings within the process industry, such as [54,56]. Although deriving an analytical expression for calculating the maximum overpressure was not part of the scope of this article, the results did indicate an underlying potential for deriving such an equation for applications in a traffic environment. Indeed, if the distance covered by the flame across the transverse direction, L_p, is defined as described by Eq. (20), a strong linear relationship between the maximum overpressure (see Fig. 10) and $L_p^{2.75}$ can be demonstrated, with $R^2 > 0.999$. Remarkably, a similar relationship between L_p and maximum overpressure in explosion experiments in 3D configurations was found in [54]. This highlights the significance of factor D to the explosion strength. It also shows that it would be beneficial to further explore this topic in future research.

$$L_p = D \cdot b_{car} + (D - 1) \cdot A \tag{20}$$

To enable consideration of directional blast effects in the near field, the approach distinguishes between a localised source of greater strength but lower energy content (located right outside the congested region) and a global explosion (which governs the resulting load in the far field). Thus, the approach addresses one of the most important

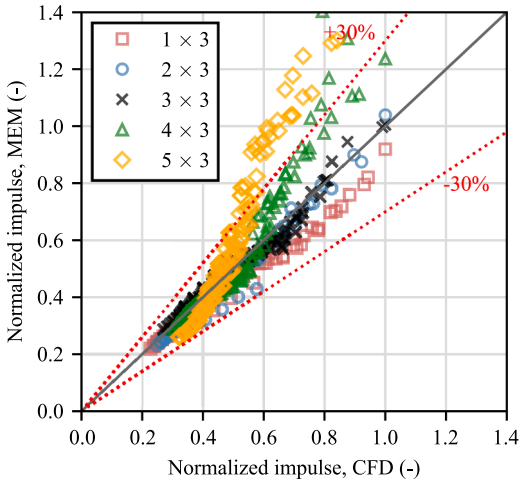

Fig. 23. Comparison of the peak impulse prediction in the reference scenarios with a mixture of methane and air.
Scenarios II-19 to II-23.

weaknesses of the MEM and other similar methods; namely, the assumption of point-symmetrical blast propagation. This modification will be particularly relevant for stronger explosions and for structures that are immediately next to the road or carpark.

Finally, the proposed strength class numbers are conservative in that they were calculated by maximising the effect of all other parameters and assuming a constant stoichiometric concentration. However, they are still less conservative than assuming the most severe explosion strength, which is the default choice in uncertain scenarios [73]. Moreover, if the proposed approach results in unacceptably high blast loading, there is still the possibility of reducing it if the real distance between the vehicles is not equal to the critical value found here (1.5 m). The results also indicated that it may be possible to decrease the overall size of the blast source in scenarios with one or two rows of vehicles in the transverse direction. Hence, it would be helpful to investigate further and introduce these aspects into the guidelines in future research work.

7. Conclusions

This study presents recommendations for implementing the TNO Multi-Energy Method (MEM) for simplified estimates of the peak overpressure and peak positive impulse generated by VCEs in traffic environments based on CFD calculations. Specifically, the proposed guidelines inform the users regarding the choice of strength class and size of the equivalent source of blast (that is, the gas volume contributing to strong blast generation) based on the geometrical conditions of the scenarios. The scenarios of interest consisted of several vehicles on an open road engulfed by a propane-air mixture with a stoichiometric concentration. These scenarios were defined by the distance between vehicles, the dimensions of the gas cloud in the horizontal and vertical directions, and the number of vehicles in the transverse (perpendicular to the direction of traffic) and longitudinal (parallel to the direction of traffic) directions.

Results from CFD analyses were used to formulate a relationship between the strength class in the MEM and the geometrical conditions of the scenarios of interest. While all the studied parameters affected the blast strength to some extent, it was found that the strength class could be reasonably estimated based mainly on the number of vehicles in the transverse direction. However, the effect of the number of vehicles in the transverse direction was found to diminish in elongated, transverse configurations, likely due to a greater influence of side venting. This could be considered by correcting the strength class based on the ratio between the number of vehicles in the transverse and longitudinal directions. To make this simplification applicable to different scenarios, the influence of all other parameters was maximised in the scenarios used for fitting the MEM to the CFD results.

The study showed that the influence of the gas volume on the resulting explosion levelled off after a certain volume. That is, a further increase of the gas volume from this point did not result in a noticeable increase in peak overpressure or peak impulse. This property was used to formulate recommendations for estimating the size of the equivalent blast source to be used in the MEM. Moreover, the proposed approach distinguishes between a global source and a localised one, which enables directional blast effects to be considered.

The peak impulse prediction using the MEM (according to the derived recommendations) was shown to have very good agreement with the CFD results. However, achieving acceptable predictions of peak overpressure was more challenging, mainly due to the contrast between the assumption of point-symmetrical blast wave propagation in the MEM and the inherent asymmetry of the scenarios of interest, plus the relatively large steps between strength classes in the MEM. However, it was possible to obtain reasonable and conservative predictions of peak overpressure. The prediction with the MEM generally improved further from the explosion centre.

Ethics Statement

Not applicable because this work does not involve the use of animal or human subjects.

CRediT authorship contribution statement

Fabio Lozano: Writing – original draft, Visualization, Validation, Software, Methodology, Investigation, Formal analysis, Conceptualization. **Morgan Johansson:** Writing – review & editing, Supervision, Project administration, Methodology, Funding acquisition, Conceptualization. **Joosef Leppänen:** Writing – review & editing, Supervision, Project administration, Methodology, Funding acquisition, Conceptualization. **Mario Plos:** Writing – review & editing, Supervision, Methodology, Conceptualization.

Declaration of interest statement

The authors declare that they have no known competing financial interests or personal relationships that could have appeared to influence the work reported in this paper.

Acknowledgments

This work was financed by the Swedish Transport Administration, the Swedish Fortifications Agency, and the Swedish Civil Contingencies Agency. The authors are grateful for their support.

The calculations were performed on two high performance computing (HPC) clusters: i) *Vera*, provided by Chalmers e-Commons at Chalmers; ii) *Tetralith,* provided by the National Academic Infrastructure for Supercomputing in Sweden (NAISS) and the Swedish National Infrastructure for Computing (SNIC).

Appendix A. Brief description of the TNO Multi-Energy Method

The MEM was originally proposed by van den Berg [42] and has been complemented by such works as [54,78,79]. The method assumes that a strong blast can only be produced in those regions within the gas cloud that is partially congested or confined, whereas the remaining unconfined part of the cloud does not contribute significantly to overpressure generation. The blast wave parameters are obtained from blast charts for side-on peak overpressure, ΔP^+, and positive-phase duration, t^+, as a function of the energy-scaled distance, $\overline{R}$. The energy-scaled distance depends on the estimated combustion energy released by the explosion, ϵ. The method associates the combustion energy with the gas volume at the blast source, V_{gas}, by means of Eq. (A.1). The parameter ϵ_0 is the specific heat of combustion taken as 3.5 MJ/m^3, which is a representative value of the specific heats of combustion of most common hydrocarbons. The energy-scaled distance, $\overline{R}$, is calculated using Eq. (A.2), in which R is the stand-off distance and P_0 is the ambient pressure (set to 101.3 kPa in this study).

$$\epsilon = \epsilon_0 \cdot V_{gas} \tag{A.1}$$

$$\overline{R} = R \cdot \left(\frac{e}{P_0}\right)^{-\frac{1}{3}} \tag{A.2}$$

Fig. A.1(a) gives the charts for ΔP^+, containing a set of 10 curves representing different strength classes, S. Explosions with the lowest strength classes produce low overpressure values. Conversely, the highest strength class corresponds to the detonation of the fuel-air mixture. The strength class is a site-specific parameter that depends on conditions such as the degree of confinement and obstruction, fuel type, venting and energy of ignition.

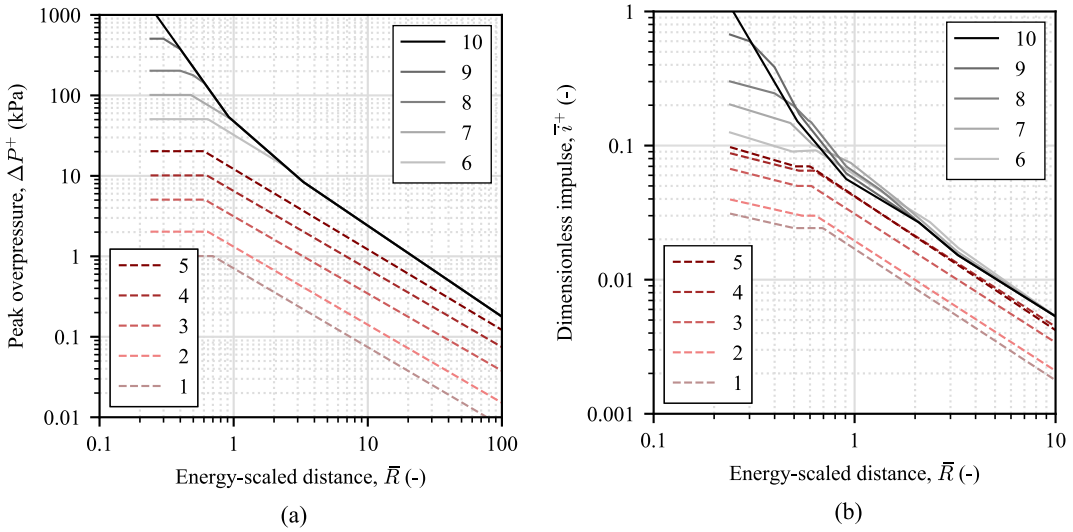

Fig. A.1. Charts for (a) side-on peak overpressure and (b) dimensionless positive impulse as a function of the energy-scaled distance and strength class according to the MEM. Plotted with equations provided in [80].

The MEM does not provide a chart for directly determining the positive peak impulse, i^+. However, i^+ can be determined from ΔP^+ and t^+ if the shape of the overpressure-time history is known or assumed. For a triangular shape, the peak impulse can be calculated using Eq. (A.3) [73]. The dimensionless peak impulse, $\overline{i}^+$, can also be extracted from Fig. A.1(b), which has been created assuming a triangular waveform. The peak impulse is calculated from the dimensionless value using Eq. (A.4), in which c_0 is the ambient sound velocity (340.3 m/s).

$$i^+ = \frac{\Delta P^+ \cdot t^+}{2} \tag{A.3}$$

$$i^+ = \overline{i}^+ \cdot {c_0}^{-1} \cdot {P_0}^{2/3} \cdot e^{1/3} \tag{A.4}$$

Appendix B. Summary of the studied scenarios

Table B.1
Scenarios used in the parametric study. The gas cloud consists of a mixture of propane and air with an equivalence ratio of 1.05.

Scenario	A (m)	B (m)	C (m)	D (-)	E (-)	Ignition point (m)
I-01*	0.5	2.0	1.8	3	3	(7.7, 0.0, 0.18)
I-02	1.0	2.0	1.8	3	3	(8.2, 0.0, 0.18)
I-03	1.5	2.0	1.8	3	3	(8.7, 0.0, 0.18)
I-04	2.0	2.0	1.8	3	3	(9.2, 0.0, 0.18)
I-05	2.5	2.0	1.8	3	3	(9.7, 0.0, 0.18)
I-06	0.5	0.1	1.8	1	1	(2.4, 0.0, 0.18)
I-07	0.5	0.5	1.8	1	1	(2.4, 0.0, 0.18)
I-08	0.5	1.0	1.8	1	1	(2.4, 0.0, 0.18)
I-09	0.5	4.0	1.8	1	1	(2.4, 0.0, 0.18)
I-10	0.5	8.0	1.8	1	1	(2.4, 0.0, 0.18)
I-11	0.5	0.1	1.8	3	3	(7.7, 0.0, 0.18)
I-12	0.5	0.5	1.8	3	3	(7.7, 0.0, 0.18)
I-13	0.5	1.0	1.8	3	3	(7.7, 0.0, 0.18)
I-14	0.5	4.0	1.8	3	3	(7.7, 0.0, 0.18)
I-15	0.5	8.0	1.8	3	3	(7.7, 0.0, 0.18)
I-16	0.5	2.0	0.9	1	1	(2.4, 0.0, 0.18)
I-17	0.5	2.0	2.7	1	1	(2.4, 0.0, 0.18)
I-18	0.5	2.0	3.6	1	1	(2.4, 0.0, 0.18)
I-19	0.5	2.0	4.5	1	1	(2.4, 0.0, 0.18)
I-20	0.5	2.0	0.9	3	3	(7.7, 0.0, 0.18)
I-21	0.5	2.0	2.7	3	3	(7.7, 0.0, 0.18)
I-22	0.5	2.0	3.6	3	3	(7.7, 0.0, 0.18)

(*continued on next page*)

Table B.1 (*continued*)

I-23	0.5	2.0	4.5	3	3	(7.7, 0.0, 0.18)
I-24	0.5	2.0	1.8	1	1	(2.4, 0.0, 0.18)
I-25	0.5	2.0	1.8	2	1	(2.4, 0.0, 0.18)
I-26	0.5	2.0	1.8	3	1	(2.4, 0.0, 0.18)
I-27	0.5	2.0	1.8	4	1	(2.4, 0.0, 0.18)
I-28	0.5	2.0	1.8	5	1	(2.4, 0.0, 0.18)
I-29	0.5	2.0	1.8	6	1	(2.4, 0.0, 0.18)
I-30	0.5	2.0	1.8	1	2	(2.4, 0.0, 0.18)
I-31	0.5	2.0	1.8	2	2	(2.4, 0.0, 0.18)
I-32	0.5	2.0	1.8	3	2	(2.4, 0.0, 0.18)
I-33	0.5	2.0	1.8	4	2	(2.4, 0.0, 0.18)
I-34	0.5	2.0	1.8	5	2	(2.4, 0.0, 0.18)
I-35	0.5	2.0	1.8	1	3	(7.7, 0.0, 0.18)
I-36	0.5	2.0	1.8	2	3	(7.7, 0.0, 0.18)
I-37	0.5	2.0	1.8	4	3	(7.7, 0.0, 0.18)
I-38	0.5	2.0	1.8	5	3	(7.7, 0.0, 0.18)

* Base scenario for the parametric study.

Table B.2
Scenarios used for fitting and validation purposes.

Scenario	Fuel	Equivalence ratio (-)	*A* (m)	*B* (m)	*C* (m)	*D* (-)	*E* (-)	Ignition point (m)	Label
II-01*	Propane	1.05	1.5	4.0	3.6	1	3	(8.7, 0.0, 0.18)	1 × 3
II-02*	Propane	1.05	1.5	4.0	3.6	2	3	(8.7, 0.0, 0.18)	2 × 3
II-03*	Propane	1.05	1.5	4.0	3.6	3	3	(8.7, 0.0, 0.18)	3 × 3
II-04*	Propane	1.05	1.5	4.0	3.6	4	3	(8.7, 0.0, 0.18)	4 × 3
II-05*	Propane	1.05	1.5	4.0	3.6	5	3	(8.7, 0.0, 0.18)	5 × 3
II-06	Propane	1.05	1.5	4.0	3.6	2	1	(2.4, 0.0, 0.18)	2 × 1
II-07	Propane	1.05	1.5	4.0	3.6	3	1	(2.4, 0.0, 0.18)	3 × 1
II-08	Propane	1.05	1.5	4.0	3.6	4	1	(2.4, 0.0, 0.18)	4 × 1
II-09	Propane	1.05	1.5	4.0	3.6	5	1	(2.4, 0.0, 0.18)	5 × 1
II-10	Propane	1.05	1.5	4.0	3.6	2	2	(2.4, 0.0, 0.18)	2 × 2
II-11	Propane	1.05	1.5	4.0	3.6	3	2	(2.4, 0.0, 0.18)	3 × 2
II-12	Propane	1.05	1.5	4.0	3.6	4	2	(2.4, 0.0, 0.18)	4 × 2
II-13	Propane	1.05	1.5	4.0	3.6	5	2	(2.4, 0.0, 0.18)	5 × 2
II-14	Propane	1.05	1.5	4.0	3.6	2	4	(8.7, 0.0, 0.18)	2 × 4
II-15	Propane	1.05	1.5	4.0	3.6	2	5	(15, 0.0, 0.18)	2 × 5
II-16	Propane	1.05	1.5	4.0	3.6	2	6	(15, 0.0, 0.18)	2 × 6
II-17	Propane	1.05	1.5	4.0	3.6	3	4	(8.7, 0.0, 0.18)	3 × 4
II-18	Propane	1.05	1.5	4.0	3.6	3	5	(15, 0.0, 0.18)	3 × 5
II-19	Methane	1.08	1.5	4.0	3.6	1	3	(8.7, 0.0, 0.18)	1 × 3
II-20	Methane	1.08	1.5	4.0	3.6	2	3	(8.7, 0.0, 0.18)	2 × 3
II-21	Methane	1.08	1.5	4.0	3.6	3	3	(8.7, 0.0, 0.18)	3 × 3
II-22	Methane	1.08	1.5	4.0	3.6	4	3	(8.7, 0.0, 0.18)	4 × 3
II-23	Methane	1.08	1.5	4.0	3.6	5	3	(8.7, 0.0, 0.18)	5 × 3

* Reference scenarios used for the initial fitting of the strength class in the MEM to the CFD results.

Appendix C. The approach in practice

Overview

This article proposes an approach to applying MEM to estimating the blast load from gas explosions in a traffic environment. This section presents the concept in its entirety to facilitate understanding and implementation of the approach. Specifically, the study gives guidance for estimating the size of the equivalent blast source (which relates to the energy content) and explosion strength. Moreover, the presented approach includes a strategy for dealing with the directionality of the blast load in the near field. Our recommendations are intended for hydrocarbon gases with low or medium reactivity (such as propane) in scenarios in which combustion evolves as a deflagration. Furthermore, the method assumes that there is sufficient flammable material to engulf the entire group of vehicles under consideration. The influence of the fuel reactivity could be included by scaling the explosion characteristics of a propane-air mixture to the conditions of the fuel type of interest. Explosion scenarios with major potential for direct detonation or deflagration-to-detonation transition (DDT) are beyond the scope of the proposed approach.

Equivalent blast source

The initial step involves estimating the volume of the equivalent blast source, V_{source}. This volume is then used to calculate the combustion energy released by the explosion. The equivalent source is assumed to be a gas cloud with uniform stoichiometric concentration. In the vertical direction, the equivalent cloud is assumed to extend 1.0 m beyond the roof of the vehicles. In the horizontal plane, the equivalent cloud is assumed to extend 2.0 m beyond the edge of the group of vehicles in both directions. Therefore, if the vehicles are arranged in a rectangular pattern, the equivalent cloud will take the shape of a rectangular cuboid, as shown in Fig. C.1. In such a case, the total gas volume is calculated by Eq. (C.1), in which V_{car} is the volume occupied by one vehicle and n_{car} is the total number of vehicles within the gas cloud.

$$V_{source} = l_{source} \cdot b_{source} \cdot h_{source} - n_{car} \cdot V_{car} \tag{C.1}$$

To determine the blast load in the near field, the blast source is divided into a localised source and a global one. The near field is defined as the

region within an energy-scaled distance equal to 0.6 from the centre of the vehicle cluster. To find the boundary between the near field and the far field, the distance is scaled with regard to the total gas volume, V_{source}. The localised source is placed just outside the group of vehicles and can be viewed as an external explosion of greater initial strength but less energy content than the global explosion. The gas volume mobilised by the localised explosion, V_{lc}, is coupled to the size of the recirculation zone on the wake of the vehicle group. This volume is estimated for a perpendicular path crossing a vehicle, as shown in Fig. C.1(b). For this path, V_{lc} is taken as the product of the projected area of the long side of the vehicle and the width of the cloud outside the congested region (2.0 m). For the geometry of the vehicle in this study, $V_{lc} = 1.5\ \text{m} \times 4.8\ \text{m} \times 2.0\ \text{m} = 14.4\ \text{m}^3$. The distance from the localised source to the studied point, R_{lc}, is measured from the edge of the vehicle group. The localised source is centred around the evaluated path. That is, its location is shifted as the angle of the evaluated path changes. However, for the sake of simplicity, the volume of the localised source determined for a perpendicular path is used for all angles. The localised source need only be considered in the critical direction, as defined in Fig. C.1 (c).

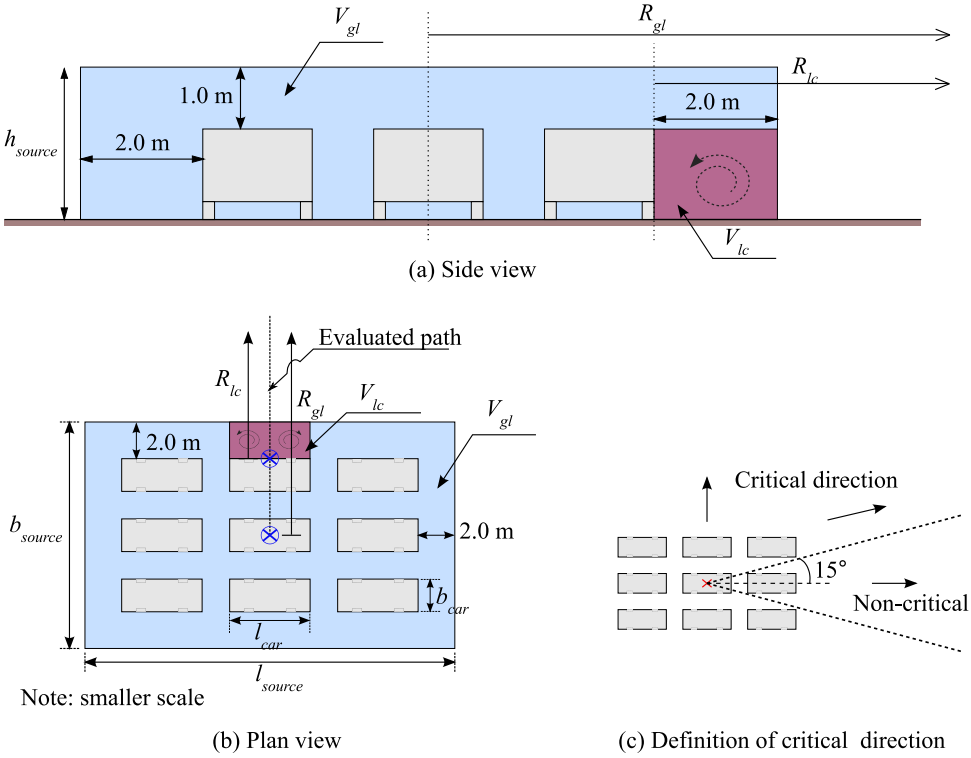

Fig. C.1. Schematic representation of the equivalent blast source due to a group of vehicles. The purple region gives the volume corresponding to the localised source for a perpendicular path: (a) Side view; (b) Plan view; (c) Definition of critical direction for the localised source.

The volume of the global source is equal to the difference between the total and localised gas volume, $V_{gl} = V_{source} - V_{lc}$. The distance from the global source, R_{gl}, is measured from the centre of the configuration.

To calculate the blast load in the far field (energy-scaled distance > 0.6), only the global explosion needs to be considered. In such a case, the volume of the global source equals the total gas volume: $V_{gl} = V_{source}$.

In configurations elongated in the direction of traffic (such as a long queue on a road), the length of the equivalent gas cloud should be limited to $l_{source.max} = 2.5 \bullet b_{source}$, see Fig. 20.

Strength class at the source

The strength class, S, at the blast source depends primarily on the number of vehicles in the transverse direction. Table C.1 gives the strength class as a function of the number of vehicles in the transverse direction, both for the localised explosion, S_{lc}, and for the global explosion, S_{gl}. The maximum overpressure for each strength class according to the MEM, P_{MEM}, is also given in the table.

Table C.1
Strength class for the localised and global explosion.

No. of vehicles in the transverse direction	Localised source		Global source	
	S_{lc} (-)	P_{MEM} (kPa)	S_{gl} (-)	P_{MEM} (kPa)
1	4	10	4	10
2	6	50	5	20
3	7	100	6	50
4	8	200	7	100
5	9	500	8	200
≥ 6	≥ 9	≥ 500	≥ 8	≥ 200

In configurations that are long and narrow in the transverse direction, the strength class should be reduced, as given in Table C.2.

Table C.2
Strength class for the localised and global explosion for long and narrow configurations.

No. of vehicles in the transverse direction	One vehicle in the direction of traffic		Two vehicles in the direction of traffic	
	Localised source	Global source	Localised source	Global source
	S_{lc} (-)	S_{gl} (-)	S_{lc} (-)	S_{gl} (-)
3	7	5	7	6
4	7	6	7	7
5	7	6	8	7
≥6	≥7	≥6	≥8	≥7

Determination of blast wave parameters

At a given point, the side-on peak overpressure (ΔP^+_{lc}, ΔP^+_{gl}) and positive-phase duration (t^+_{lc}, t^+_{gl}) due to the localised and global explosions are determined separately according to the standard MEM procedure. From these, the peak impulse (i^+_{lc}, i^+_{gl}) is determined by assuming a triangular waveform for the overpressure-time history using Eqs. (C.2) and (C.3). Alternatively, the peak impulse can be extracted from Fig. A.1(b). Finally, the dominant peak overpressure, ΔP^+, and the total peak impulse, i^+, are calculated using Eqs. (C.4) and (C.5).

$$i^+_{lc} = \frac{\Delta P^+_{lc} \cdot t^+_{lc}}{2} \tag{C.2}$$

$$i^+_{gl} = \frac{\Delta P^+_{gl} \cdot t^+_{gl}}{2} \tag{C.3}$$

$$\Delta P^+ = \max\left(\Delta P^+_{lc}, \Delta P^+_{gl}\right) \tag{C.4}$$

$$i^+ = i^+_{lc} + i^+_{gl} \tag{C.5}$$

Fuel scaling

The approach can be used directly for propane-air mixtures or other mixtures with similar reactivity. However, for other fuel-air mixtures, the calculated values of peak overpressure and impulse need to be corrected by a factor κ (given by Eq. (C.6)), in which U_0 and α are the laminar burning speed and the expansion ratio of the relevant mixture.

$$\kappa = \left[\frac{U_0 \cdot (\alpha - 1)}{(0.464\ \text{m/s}) \cdot (8.09 - 1)}\right]^{2.72} \tag{C.6}$$

References

[1] F.I. Khan, S.A. Abbasi, Major accidents in process industries and an analysis of causes and consequences, J. Loss Prev. Process Ind. 12 (1999) 361–378, https://doi.org/10.1016/S0950-4230(98)00062-X.

[2] T. Abbasi, S.A. Abbasi, The boiling liquid expanding vapour explosion (BLEVE): Mechanism, consequence assessment, management, J. Hazard. Mater. 141 (2007) 489–519, https://doi.org/10.1016/j.jhazmat.2006.09.056.

[3] J. Yang, F. Li, J. Zhou, L. Zhang, L. Huang, J. Bi, A survey on hazardous materials accidents during road transport in China from 2000 to 2008, J. Hazard. Mater. 184 (2010) 647–653, https://doi.org/10.1016/j.jhazmat.2010.08.085.

[4] Y. Kang, Z. Wu, S. Ma, M. Zhao, W. Li, CFD-based assessment and visualization of the failure consequences of LPG tankers, J. Loss Prev. Process Ind. 82 (2023) 105008, https://doi.org/10.1016/j.jlp.2023.105008.

[5] S. Lyu, S. Zhang, X. Huang, S. Peng, J. Li, Investigation and modeling of the LPG tank truck accident in Wenling, China, Process Saf. Environ. Prot. 157 (2022) 493–508, https://doi.org/10.1016/j.psep.2021.10.022.

[6] D. Yang, K. Peng, J. Zheng, B. Xie, J. Wang, B. Xu, F. Li, Consequences analysis of the LPG tank truck traffic accident: a case study of the Wenling explosion accident, J. Loss Prev. Process Ind. 87 (2024) 105228, https://doi.org/10.1016/j.jlp.2023.105228.

[7] N. Bariha, I.M. Mishra, V.C. Srivastava, Fire and explosion hazard analysis during surface transport of liquefied petroleum gas (LPG): A case study of LPG truck tanker accident in Kannur, Kerala, India, J. Loss Prev. Process Ind. 40 (2016) 449–460, https://doi.org/10.1016/j.jlp.2016.01.020.

[8] J. Li, H. Hao, Numerical simulation of medium to large scale BLEVE and the prediction of BLEVE's blast wave in obstructed environment, Process Saf. Environ. Prot. 145 (2021) 94–109, https://doi.org/10.1016/j.psep.2020.07.038.

[9] G. Cocchi, The Bologna LPG BLEVE, in: Proceedings of the 28th International Colloquium on the Dynamics of Explosions and Reactive Systems, Napoli, 2022.

[10] R. Bubbico, C. Ferrari, B. Mazzarotta, Risk analysis of LPG transport by road and rail, J. Loss Prev. Process Ind. 13 (2000) 27–31, https://doi.org/10.1016/S0950-4230(99)00057-1.

[11] J. Casal, Evaluation of the Effects and Consequences of Major Accidents in Industrial Plants, 2nd ed., Elsevier, 2017.

[12] D. Bjerketvedt, J.R. Bakke, K. van Wingerden, Gas Explosion Handbook, Gexcon, Bergen, 1992.

[13] Y. Shi, H. Hao, Z.-X. Li, Numerical derivation of pressure–impulse diagrams for prediction of RC column damage to blast loads, Int. J. Impact Eng. 35 (2008) 1213–1227, https://doi.org/10.1016/j.ijimpeng.2007.09.001.

[14] A. Sari, B. Sayin, Risk-based explosion hazard analysis and building upgrades in industrial facilities to prevent blast failures, Process Saf. Prog. 41 (2022) 14–24, https://doi.org/10.1002/prs.12278.

[15] G. Momferatos, S.G. Giannissi, I.C. Tolias, A.G. Venetsanos, A. Vlyssides, N. Markatos, Vapor cloud explosions in various types of confined environments: CFD analysis and model validation, J. Loss Prev. Process Ind. 75 (2022) 104681, https://doi.org/10.1016/j.jlp.2021.104681.

[16] D.S.N. Abg Shamsuddin, A.F. Mohd Fekeri, A. Muchtar, F. Khan, B.C. Khor, B. H. Lim, M.I. Rosli, M.S. Takriff, Computational fluid dynamics modelling approaches of gas explosion in the chemical process industry: a review, Process Saf. Environ. Prot. 170 (2023) 112–138, https://doi.org/10.1016/j.psep.2022.11.090.

[17] R. Shen, Z. Jiao, T. Parker, Y. Sun, Q. Wang, Recent application of computational fluid dynamics (CFD) in process safety and loss prevention: a review, J. Loss Prev. Process Ind. 67 (2020) 104252, https://doi.org/10.1016/j.jlp.2020.104252.

[18] Z. Yan, Development in comprehensive CFD simulation of fire and explosion, J. Saf. Sci. Resil. 4 (2023) 203–219, https://doi.org/10.1016/j.jnlssr.2022.12.003.

[19] S. Mishra, K.B. Mishra, Numerical study of large-scale LNG vapour cloud explosion in an unconfined space, Process Saf. Environ. Prot. 149 (2021) 967–976, https://doi.org/10.1016/j.psep.2021.03.034.

[20] Q. Hu, X. Qian, X. Shen, Q. Zhang, C. Ma, L. Pang, Y. Liang, H. Feng, M. Yuan, Investigations on vapor cloud explosion hazards and critical safe reserves of LPG tanks, J. Loss Prev. Process Ind. 80 (2022) 104904, https://doi.org/10.1016/j.jlp.2022.104904.

[21] M.H. Bae, J.K. Paik, Effects of structural congestion and surrounding obstacles on the overpressure loads in explosions: experiment and CFD simulations, Sh. Offshore Struct. 13 (2018) 165–180, https://doi.org/10.1080/17445302.2017.1347978.

[22] X. Li, R. Abbassi, G. Chen, Q. Wang, Modeling and analysis of flammable gas dispersion and deflagration from offshore platform blowout, Ocean Eng. 201 (2020) 107146, https://doi.org/10.1016/j.oceaneng.2020.107146.

[23] D. Li, Q. Zhang, Q. Ma, S. Shen, J. Chen, S. Ren, Influence of built-in obstacles on unconfined vapor cloud explosion, J. Loss Prev. Process Ind. 43 (2016) 449–456, https://doi.org/10.1016/j.jlp.2016.07.007.

[24] J. Li, G. Ma, M. Abdel-jawad, H. Hao, Evaluation of gas explosion overpressures at configurations with irregularly arranged obstacles, J. Perform. Constr. Facil. 29 (2014), https://doi.org/10.1061/(ASCE)CF.1943-5509.0000678.

[25] S. Zhang, Q. Zhang, Influence of geometrical shapes on unconfined vapor cloud explosion, J. Loss Prev. Process Ind. 52 (2018) 29–39, https://doi.org/10.1016/j.jlp.2018.01.004.

[26] T. Skjold, H. Hisken, S. Lakshmipathy, G. Atanga, M. Carcassi, M. Schiavetti, J. R. Stewart, A. Newton, J.R. Hoyes, I.C. Tolias, A.G. Venetsanos, O.R. Hansen, J. Geng, A. Huser, S. Helland, R. Jambut, K. Ren, A. Kotchourko, T. Jordan, J. Daubech, G. Lecocq, A.G. Hanssen, C. Kumar, L. Krumenacker, S. Jallais, D. Miller, C.R. Bauwens, Blind-prediction: Estimating the consequences of vented hydrogen deflagrations for homogeneous mixtures in 20-foot ISO containers, Int. J. Hydrog. Energy 44 (2019) 8997–9008, https://doi.org/10.1016/j.ijhydene.2018.06.191.

[27] I.C. Tolias, J.R. Stewart, A. Newton, J. Keenan, D. Makarov, J.R. Hoyes, V. Molkov, A.G. Venetsanos, Numerical simulations of vented hydrogen deflagration in a medium-scale enclosure, J. Loss Prev. Process Ind. 52 (2018) 125–139, https://doi.org/10.1016/j.jlp.2017.10.014.

[28] E. Vyazmina, S. Jallais, L. Krumenacker, A. Tripathi, A. Mahon, J. Commanay, S. Kudriakov, E. Studer, T. Vuillez, F. Rosset, Vented explosion of hydrogen/air mixture: An intercomparison benchmark exercise, Int. J. Hydrog. Energy 44 (2019) 8914–8926, https://doi.org/10.1016/j.ijhydene.2018.07.195.

[29] E. Vyazmina, S. Jallais, Validation and recommendations for FLACS CFD and engineering approaches to model hydrogen vented explosions: Effects of concentration, obstruction vent area and ignition position, Int. J. Hydrog. Energy 41 (2016), https://doi.org/10.1016/j.ijhydene.2016.05.189.

[30] O.R. Hansen, P. Hinze, D. Engel, S. Davis, Using computational fluid dynamics (CFD) for blast wave predictions, J. Loss Prev. Process Ind. 23 (2010) 885–906, https://doi.org/10.1016/j.jlp.2010.07.005.

[31] O.R. Hansen, D.M. Johnson, Improved far-field blast predictions from fast deflagrations, DDTs and detonations of vapour clouds using FLACS CFD, J. Loss Prev. Process Ind. 35 (2015) 293–306, https://doi.org/10.1016/j.jlp.2014.11.005.

[32] J. Li, H. Hao, Internal and external pressure prediction of vented gas explosion in large rooms by using analytical and CFD methods, J. Loss Prev. Process Ind. 49 (2017) 367–381, https://doi.org/10.1016/j.jlp.2017.08.002.

[33] D. Baraldi, A. Kotchourko, A. Lelyakin, J. Yanez, P. Middha, O.R. Hansen, A. Gavrikov, A. Efimenko, F. Verbecke, D. Makarov, V. Molkov, An inter-comparison exercise on CFD model capabilities to simulate hydrogen deflagrations in a tunnel, Int. J. Hydrog. Energy 34 (2009) 7862–7872, https://doi.org/10.1016/j.ijhydene.2009.06.055.

[34] Y.Z. Li, Study of fire and explosion hazards of alternative fuel vehicles in tunnels, Fire Saf. J. 110 (2019) 102871, https://doi.org/10.1016/j.firesaf.2019.102871.

[35] P. Middha, O.R. Hansen, Using computational fluid dynamics as a tool for hydrogen safety studies, J. Loss Prev. Process Ind. 22 (2009) 295–302, https://doi.org/10.1016/j.jlp.2008.10.006.

[36] C.W. To, W.K. Chow, F.M. Cheng, Numerical studies on explosion hazards of vehicles using clean fuel in short vehicular tunnels, Tunn. Undergr. Space Technol. 107 (2021) 103649, https://doi.org/10.1016/j.tust.2020.103649.

[37] I.C. Tolias, A.G. Venetsanos, N. Markatos, C.T. Kiranoudis, CFD modeling of hydrogen deflagration in a tunnel, Int. J. Hydrog. Energy 39 (2014) 20538–20546, https://doi.org/10.1016/j.ijhydene.2014.03.232.

[38] W. Li, X. Shen, Z. Huang, T. Mao, Q. Hu, C. Ma, Study of leakage and explosion hazard characteristics of a compressed natural gas at a gas station, J. Eng. Phys. Thermophy. 97 (2024) 387–396, https://doi.org/10.1007/s10891-024-02904-3.

[39] D. Makarov, F. Verbecke, V. Molkov, O. Roe, M. Skotenne, A. Kotchourko, A. Lelyakin, J. Yanez, O. Hansen, P. Middha, S. Ledin, D. Baraldi, M. Heitsch, A. Efimenko, A. Gavrikov, An inter-comparison exercise on CFD model capabilities to predict a hydrogen explosion in a simulated vehicle refuelling environment, Int. J. Hydrog. Energy 34 (2009) 2800–2814, https://doi.org/10.1016/j.ijhydene.2008.12.067.

[40] C. Zhou, Z. Yang, G. Chen, X. Li, Optimizing hydrogen refueling station layout based on consequences of leakage and explosion accidents, Int. J. Hydrog. Energy 54 (2024) 817–836, https://doi.org/10.1016/j.ijhydene.2023.09.210.

[41] F. Lozano. Explosions in urban environments: Modelling of gas explosions and risk of premature shear failure in reinforced concrete structures, Lic. Thesis, Chalmers University of Technology, Gothenburg, 2023.

[42] A.C. van den Berg, The multi-energy method: a framework for vapour cloud explosion blast prediction, J. Hazard. Mater. 12 (1985) 1–10, https://doi.org/10.1016/0304-3894(85)80022-4.

[43] Q.A. Baker, M.J. Tang, E.A. Scheier, G.J. Silva, Vapor cloud explosion analysis, Process Saf. Prog. 15 (1996) 106–109, https://doi.org/10.1002/prs.680150211.

[44] M.J. Tang, Q.A. Baker, A new set of blast curves from vapor cloud explosion, Process Saf. Prog. 18 (1999) 235–240, https://doi.org/10.1002/prs.680180412.

[45] J.S. Puttock. Fuel gas explosions guidelines: the congestion assessment method, in: 2nd European Conference on Major Hazards On- and Off-Shore, Manchester, 1995.

[46] S. Li, Z. Liu, Y. Zhao, M. Li, P. Li, Flame propagation and overpressure characteristics of methane-hydrogen-mixed cloud explosion in unconfined area: experimental and model study, Process Saf. Environ. Prot. 197 (2025) 106940, https://doi.org/10.1016/j.psep.2025.106940.

[47] E.D. Mukhim, T. Abbasi, S.M. Tauseef, S.A. Abbasi, A method for the estimation of overpressure generated by open air hydrogen explosions, J. Loss Prev. Process Ind. 52 (2018) 99–107, https://doi.org/10.1016/j.jlp.2018.01.009.

[48] S. Yang, W. Sun, Q. Fang, Y. Yang, C. Xia, Q. Bao, Investigation of a practical load model for a natural gas explosion in an unconfined space, J. Saf. Sci. Resil. 3 (2022) 209–221, https://doi.org/10.1016/j.jnlssr.2022.03.004.

[49] D. Chen, C. Wu, J. Li, K. Liao, An overpressure-time history model of methane-air explosion in tunnel-shape space, J. Loss Prev. Process Ind. 82 (2023) 105004, https://doi.org/10.1016/j.jlp.2023.105004.

[50] J. Li, F. Hernandez, H. Hao, Q. Fang, H. Xiang, Z. Li, X. Zhang, L. Chen, Vented methane-air explosion overpressure calculation—A simplified approach based on CFD, Process Saf. Environ. Prot. 109 (2017) 489–508, https://doi.org/10.1016/j.psep.2017.04.025.

[51] J. Li, H. Hao, Far-field pressure prediction of a vented gas explosion from storage tanks by using new CFD simulation guidance, Process Saf. Environ. Prot. 119 (2018) 360–378, https://doi.org/10.1016/j.psep.2018.08.004.

[52] A. Sinha, J.X. Wen, A simple model for calculating peak pressure in vented explosions of hydrogen and hydrocarbons, Int. J. Hydrog. Energy 44 (2019) 22719–22732, https://doi.org/10.1016/j.ijhydene.2019.02.213.

[53] K.G. Kinsella. A rapid assessment methodology for the prediction of vapour cloud explosion overpressure, in: International Conference and Exhibition on Safety, Health and Loss Prevention in the Oil, Chemical and Process Industries, Singapore, 1993.

[54] J.B.M.M. Eggen, GAME: Development of Guidance for the Application Of The Multi-Energy Method, TNO Prins Maurits Laboratory, 1998.

[55] R. Pitblado, J. Alderman, J.K. Thomas, Facilitating consistent siting hazard distance predictions using the TNO multi-energy model, J. Loss Prev. Process Ind. 30 (2014) 287–295, https://doi.org/10.1016/j.jlp.2014.04.010.

[56] J. Li, M. Abdel-jawad, G. Ma, New correlation for vapor cloud explosion overpressure calculation at congested configurations, J. Loss Prev. Process Ind. 31 (2014) 16–25, https://doi.org/10.1016/j.jlp.2014.05.013.

[57] Y. Shi, C. Xie, Z. Li, Y. Ding, A quantitative correlation of evaluating the flame speed for the BST method in vapor cloud explosions, J. Loss Prev. Process Ind. 73 (2021) 104622, https://doi.org/10.1016/j.jlp.2021.104622.

[58] M. Johansson, A. Ansell, M. Hallgren, J. Leppänen, Inventering av kunskapsbehov i byggbranschen med hänsyn till explosioner i en förtätad stadsmiljö (Inventory of knowledge needs in the construction industry regarding explosions in densified urban environments. In Swedish), Chalmers University of Technology, Gothenburg, 2020.

[59] A.S. Gexcon, FLACS-CFD v22.1 User's Manual, 2022.

[60] O. Alvarsson, J. Jansson, Jämförelsestudie av riskbedömningar avseende vägtransport av farligt gods (Comparison study of risk analyses regarding road transport of hazardous materials. In Swedish), M.Sc. thesis, Lund University, Lund, 2016.

[61] E. Dahlén. Inventory of knowledge needs, with regard to explosion loading, in a densified urban environment, M.Sc. thesis, Chalmers University of Technology, Gothenburg, 2019.

[62] B.H. Hjertager, Computer simulation of turbulent reactive gas dynamics, MIC 5 (1984) 211–236, https://doi.org/10.4173/mic.1984.4.3.

[63] B.H. Hjertager, Computer modelling of turbulent gas explosions in complex 2D and 3D geometries, J. Hazard. Mater. 34 (1993) 173–197, https://doi.org/10.1016/0304-3894(93)85004-X.

[64] B.J. Arntzen. Modelling of turbulence and combustion for simulation of gas explosions in complex geometries, Ph.D. Thesis, NTNU: Norwegian University of Science and Technology, 1998.

[65] B. Launder, D.B. Spalding, The numerical computation of turbulent flow computer methods, Comput. Methods Appl. Mech. Eng. 3 (1974) 269–289, https://doi.org/10.1016/0045-7825(74)90029-2.

[66] J.C. Chang, S.R. Hanna, Air quality model performance evaluation, Meteorol. Atmos. Phys. 87 (2004), https://doi.org/10.1007/s00703-003-0070-7.

[67] W.M. Cox, J.A. Tikvart, A statistical procedure for determining the best performing air quality simulation model, Atmos. Environ. A. Gen. Top. 24 (1990) 2387–2395, https://doi.org/10.1016/0960-1686(90)90331-G.

[68] E.A. Papanikolaou, A.G. Venetsanos, M. Heitsch, D. Baraldi, A. Huser, J. Pujol, J. Garcia, N. Markatos, HySafe SBEP-V20: Numerical studies of release experiments inside a naturally ventilated residential garage, Int. J. Hydrog. Energy 35 (2010) 4747–4757, https://doi.org/10.1016/j.ijhydene.2010.02.020.

[69] J.R. Stewart, H.N. Phylaktou, G.E. Andrews, A.D. Burns, Evaluation of CFD simulations of transient pool fire burning rates, J. Loss Prev. Process Ind. 71 (2021) 104495, https://doi.org/10.1016/j.jlp.2021.104495.

[70] A.M. Na'inna, H.N. Phylaktou, G.E. Andrews, The acceleration of flames in tube explosions with two obstacles as a function of the obstacle separation distance, J. Loss Prev. Process Ind. 26 (2013) 1597–1603, https://doi.org/10.1016/j.jlp.2013.08.003.

[71] J.S. Puttock, T7-5 - developments in the congestion assessment method for the prediction of vapour-cloud explosions, in: H.J. Pasman, O. Fredholm, A. Jacobsson (Eds.), Loss Prevention and Safety Promotion in the Process Industries, Elsevier Science B.V., Amsterdam, 2001, pp. 1107–1133, https://doi.org/10.1016/B978-044450699-3/50026-4.

[72] A.T. Cates. Fuel gas explosion guidelines, in: Conference on Fire and Explosion Hazards, Moreton-in-Marsh, 1991.

[73] Committee for the Prevention of Disasters, Methods for the Calculation of Physical Effects ['Yellow Book'], The Hague, 2005.

[74] C.J.M. van Wingerden, Experimental Study of the Influence of Obstacles and Partial Confinement on Flame Propagation, Part II, TNO Prins Maurits Laboratory, 1984.

[75] Q. Zhang, D. Li, Comparison of the explosion characteristics of hydrogen, propane, and methane clouds at the stoichiometric concentrations, Int. J. Hydrog. Energy 42 (2017) 14794–14808, https://doi.org/10.1016/j.ijhydene.2017.04.201.
[76] P.H. Taylor, W.J.S. Hirst, The scaling of vapour cloud explosions: a fractal model for size and fuel type. 22nd International Symposium on Combustion, Seattle, 1988.
[77] W.E. Baker, P.A. Cox, J.J. Kulesz, R.A. Strehlow, P.S. Westine. Explosion Hazards and Evaluation (Fundamental Studies in Engineering), Elsevier Scientific Pub. Co, Amsterdam, 1983.
[78] A.C. van den Berg, A.L. Mos, Research to Improve Guidance on Separation Distance for the Multi-Energy Method (RIGOS), TNO Prins Maurits Laboratory, 2005.
[79] A.C. van den Berg, N.H.A. Versloot, The multi-energy critical separation distance, J. Loss Prev. Process Ind. 16 (2003) 111–120, https://doi.org/10.1016/S0950-4230(02)00112-2.
[80] M. Johansson, Beräkningsstöd: Gasexplosion i det fria (Gas explosions in the open. In Swedish), Myndigheten för Samhällsskydd och Beredskap, Karlstad, 2017.